I&EC research
Industrial & Engineering Chemistry Research

ARTICLE

pubs.acs.org/IECR

Development of Efficient Designs of Cooking Systems. II. Computational Fluid Dynamics and Optimization

Jyeshtharaj B. Joshi,[*,†,∥] Aniruddha B. Pandit,[*,†] Shirish B. Patel,[*,†,§] Rekha S. Singhal,[‡] Govind.K. Bhide,[§] Kishore V. Mariwala,[§] Bhagwat A. Devidayal,[§] Sanjay P. Danao,[†,⊥] Arijit A. Ganguli,[†] Ajitkumar S. Gudekar,[†] Prakash V. Chavan,[†] and Yogesh H. Shinde[†]

[†]Department of Chemical Engineering, Institute of Chemical Technology, Matunga, Mumbai −400019, India

[‡]Department of Food Engineering and Technology, Institute of Chemical Technology, Matunga, Mumbai −400019, India

[§]Land Research Institute, Second Floor, United India Bldg., P.M. Road, Mumbai −400001, India

[∥]Homi Bhabha National Institute, Anushaktinagar, Mumbai −400094, India

ABSTRACT: Sections 2−6 of Part I were devoted to the analysis of heat transfer characteristics of cookers. In all the experiments, only water was employed as a working medium. Now, we extend such an analysis to the actual cooking process in order to arrive at an improved cooking device. The major strategies for the optimization of energy utilization is to design appropriate insulation that has been obtained by two cover vessels. In order to select an air gap, the flow and temperature patterns in the air gap have been extensively analyzed using computational fluid dynamics (CFD). The flow pattern and heat transfer in cooking pots have also been analyzed by CFD. This has enabled us to design suitable internals for minimizing the stratification of temperature. The understanding of fluid mechanics has also given basis for selection of heat flux, gap between burner tip and cooker bottom, and temperature of flue gases leaving the cooker. Chemical engineering principles have been used for modeling and optimization. Kinetics have been obtained in batch cookers. The knowledge of kinetics, thermal mixing, axial mixing, and optimum selection of insulation have been employed for the development of continuous cookers. The continuous mode of operation also helps in saving of energy. Systematic data have been collected for the design and scale up of continuous cookers.

1. INTRODUCTION

The importance of the development of cooking devices was discussed in Part I. In Part II, we have optimized the cooking system developed in Part I. The optimization exercise consisted of selecting the appropriate rate of heat supply for burners using LPG (liquefied petroleum gas) as the fuel. The rate essentially depends upon the heat uptake rate by the cooking pots, which is supplied by condensing steam. Because the condensation heat transfer coefficient is usually very high, it was important to understand the heat uptake rate by the contents of the pot. The pots contain a mixture of water and rice (or vegetables, lentils, etc.), and the heat transfer inside the vessel occurs by natural convection. It is known that the temperature needed for the cooking of rice is about 74 °C or greater and that for lentils is 94 °C or greater. Therefore, while investigating the natural convection, it is important to ensure the spatial temperature field in such a way that the temperature at all locations is at least above the temperature levels mentioned. This consideration sets a limit on the permissible dimension (diameter in particular) of the pots and the aspect ratio. In order to increase the permissible diameter, it is important to reduce the extent of stratifications that can be made possible by providing suitable internals.

The air gap provides insulation. In the range of geometries and temperature differences under consideration, the values of the Rayleigh number may exceed the transition value and cellular convection can occur. Therefore, in order to optimize the air gap, it is important to analyze the fluid mechanics for different cooker sizes. The optimization of the air gap and the analysis of natural convection in cooling pots were comprehensively analyzed by computational fluid dynamics (CFD). In addition to the LPG burning rate, three additional parameters were optimized: (i) the gap between the burner tip and the bottom of base vessel, (ii) size of the flame (projection and spread of flame on the bottom of the base vessel) with respect to the base area, and (iii) temperature of flue gases leaving the base vessel. Further savings in energy have been implemented by developing a continuous cooker. Thus, this paper considers the ways and means of minimizing the consumption of LPG in cooking. It also considers the optimum use of solid fuel stoves and solar energy. The analysis of cookers has been restricted to foods that can be cooked by boiling or steaming.

Apart from saving fuel (energy) and thereby reducing pollution, the cooker produces food with better flavor and possibly higher nutrition values than other cooking methods. It also reduces the time a cook has to spend in the kitchen to monitoring the cooking. An attempt has also been made to improve the performance of gas burners (liquefied natural gas or LPG), solid fuel stoves, and solar energy-based heating devices. Recommendations have been made for the selection and design of these energy providers. The areas of future research work have also been highlighted and have been recommended.

Special Issue: Nigam Issue

Received: November 9, 2011
Accepted: December 19, 2011
Published: December 19, 2011

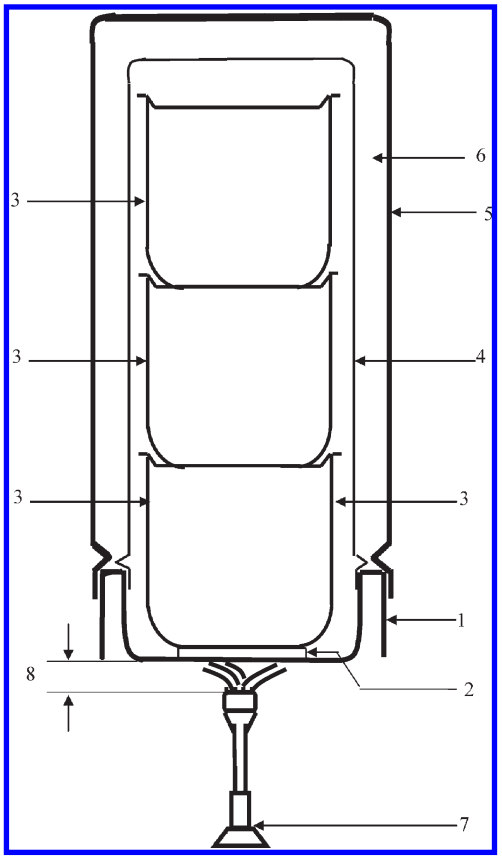

Figure 1. Schematic of cooker after phase iii development: (1) base, (2) bubble plate, (3) vessels, (4) inner cover, (5) outer cover, (6) gap between inner and outer cover, (7) burner, (8) distance between burner tip and base.

2. OPTIMIZATION USING COMPUTATIONAL FLUID DYNAMICS

2.1. Introduction. A schematic diagram of a cooker is shown in Figure 1. It essentially consists of a base vessel, support stand, set of cooking pots, metal enclosure for the pots, a second metal cover to create an air gap for providing insulation, and a gas burner. The base vessel contains water. The pots cook rice, vegetables, lentils, etc. The burner provides heat to the base vessel and boils water. The steam generated, in turn, provides heat to the cooking pots. The optimization exercise includes the selection of the appropriate rate of heat supply by the burner. The rate essentially depends upon the heat uptake rate by the cooking pots, which is supplied by condensing steam. Because the condensation heat transfer coefficient is usually very high, it was important to understand the heat uptake rate by the pot contents by natural convection. Further, the air gap (Figure 1) provides insulation.

In order to quantify the natural convection in the air gap and in the cooking pots, the technique of computational fluid dynamics (CFD) was employed. The air gap involves single-phase flow, whereas the cooking pots involve two-phase solid−liquid flows. The solid phase generally forms a fixed bed where the particle size and the voidage depend upon the extent of cooking. All of the guidelines needed for the formulation of governing equations, boundary conditions, discretization, and solution procedure are available in the published literature[3−45] .

2.2. Optimization of Air Gap between the Two Metal Covers. Minimizing thermal energy loss using an air gap as insulation has been of interest to researchers during the last many decades. Ganguli et al.[3,4] have reviewed previous work on the mathematical models from Batchelor[6] and Elder[7], experimental work from Yin et al.[8], Elsherbiny et al.[9], and Wakitani[10], and numerical studies from Newell and Schmidt[11], Korpela et al.[12], Lee and Korpela[13], Le Quéré[14], Wakitani[15], Wakitani[16], Zhao et al.[17], and Lartigue et al.[18], which have been performed on many different situations to understand the complexities of flows inside tall slender rectangular slots. The literature review suggests that in recent years a considerable amount of research has been carried out to understand the flow patterns generated in these gaps, over a wide range of Rayleigh numbers (Ra) and aspect ratios (AR), as these have been proven to be important parameters.

The conventional open pan cooking method has an efficiency of about 15−25%, while pressure cookers have net thermal efficiencies in the range of 35−40%, for instance, a pressure cooker (outer vessel aluminum) with one or more steam whistles during cooking. When one looks at conventional cooking methods, it is easily observed that the lower efficiencies are due to reasons like higher (or nonoptimum) fuel burning rates, use of excess water (especially in the case of rice cooking), and substantial and continuous heat losses to the surroundings. Pressure cookers are available up to a maximum capacity of 30 L but are rarely used beyond a size of 7−10 L because of various safety issues. In this context, the cooker developed in Sections 4−6 has been shown to possess an overall thermal efficiency in the range of 50−70%. It works at practically atmospheric pressure and is available in various capacities, from domestic (4 L) to community cooking (120 L, about 350 people). For a typical heat transfer application across a solid wall, the resistance offered by the wall and by the media on both sides determines the maximum heat flux through the wall for achieving and maintaining the required cooking temperature. In the case of cooking, heat transfer from the burning fuel, i.e., from the flame and flue gases to the cooking vessel base and effectively to the material to be cooked is determined by the area of the cooking vessel base, the temperature difference (ΔT), and the overall heat transfer coefficient (U). For a given setup and application (cooking), the heat transfer area is constant. Because the flame temperature is above 1000 °C, the value of ΔT remains practically constant during the entire period of preheating and partial cooking (30−100 °C) and subsequent cooking. In the case of cooking, U is largely dependent on the inside heat transfer coefficient (h_i). It is obvious that in the present case (as well as in the pressure cooker or any other closed cooking device), stirring is not possible (though intermittent stirring is followed in open pan cooking). This puts an upper limit on the inside heat transfer coefficient (h_i) and hence on the maximum heat uptake by the material to be cooked. By selecting an optimum ratio of cooker base to flame diameter (about 3, as determined in Section 3) and the fuel burning rate, an attempt has been made to supply heat at a rate that more or less corresponds to the heat uptake rate (decided by the internal heat transfer coefficient). Now, it is important that the heat losses to the surroundings from the side walls are also minimized. In this context, the insulation provided by the air gap between the inner and outer cover of the cooker needs to be optimized.

Let us consider an enclosed volume V_{en} surrounded by a narrow air gap that acts as insulation. Details of the air gap can be found in Figure 1. Transient temperature variation occurs inside

Table 1. Governing Equations Used for Natural Convection Problem

continuity	$\frac{\partial \rho}{\partial t} + \nabla\times(\rho\langle u_k\rangle) = 0$
momentum	$\frac{\partial(\rho\langle u_k\rangle)}{\partial t} + \nabla\times(\rho\langle u_k\rangle\langle u_k\rangle) = -\nabla\langle p\rangle + \nabla\times\tau_k + \rho \quad \tau_k = \mu_{eff}\left(\nabla\langle u_k\rangle + (\nabla\langle u_k\rangle)^T - \frac{2}{3}\mu_{eff}\nabla\times\langle u_k\rangle I\right)$
energy	$\frac{\partial(\rho\langle T\rangle)}{\partial t} + \nabla\times(\rho\langle u_k\rangle\langle T\rangle) = \nabla\times(\alpha_{eff}\langle T\rangle)$
turbulent kinetic energy	$\frac{\partial(\rho k)}{\partial t} + \langle u_k\rangle\nabla\times((\rho\langle k\rangle)) = \nabla\times\left[\left(\mu + \frac{\mu_t}{\sigma_k}\right)\nabla\times k\right] + G_k + G_b - Y_k$
	Turbulent kinetic energy (TKE) $G_k = \nu_t\lvert\bar{S}\rvert^2$ where $\lvert\bar{S}\rvert = (2\overline{S_{ij}}\,\overline{S_{ij}})^{1/2}$ and $\lvert\bar{S}\rvert = 1/2((\partial\langle u_z\rangle)/(\partial r) + (\partial\langle u_r\rangle)/(\partial z) + (\partial\langle u_\theta\rangle)/(\partial\theta))$
	Generation of turbulence due to buoyancy $G_b = -\beta g(\nu_t)/(\sigma_t)(\partial\langle T\rangle)/(\partial z)$
	Dissipation of this TKE, $Y_k = \rho\beta_\infty{}^* f_{\beta^*} k\omega$ where $\beta_\infty{}^* = 0.09, f_{\beta^*} = \begin{cases} 1, \chi_k \le 0 \\ \left[\frac{1 + 680\chi_k{}^2}{1 + 400\chi_k{}^2}\right], \chi_k > 0 \end{cases}$ and $\chi_k = (1)/(\omega^3)(\partial k)/(\partial z)(\partial\omega)/(\partial z)$
energy dissipation rate equation	$(\partial(\rho\omega))/(\partial t) + \langle u_k\rangle\nabla\times\langle\rho\omega\rangle = \nabla[(\mu + (\mu_t)/(\sigma_\omega))\nabla\omega] + G_\omega - Y_k$ Production of ω, $G_\omega = (\alpha_\infty)/(\nu_t)G_k$ where $\alpha_{\infty,1}$ and $\alpha_{\infty,2}$ are constants. $\alpha_{\infty,1} = 1$, $\alpha_{\infty,2} = 0.52$ and $Y_\omega = \rho\beta_r\omega^2$

the enclosed volume as a result of either heat supply or heat loss, and a methodology needs to be developed using existing knowledge of the extent of insulation achieved using air gaps. Here lies the main motivation for CFD simulation of the two different capacities (120 and 700 L) that have been considered. We now describe the optimization procedure briefly.

2.2.1. Computational Fluid Dynamic (CFD) Simulation. The following section describes the assumptions, governing equations, boundary conditions, and the method of solution for all of the CFD simulations carried out by Ganguli et al.[3,4] Additional details pertaining to CFD simulation can be obtained from Ekambara and Joshi[19] and Thakre and Joshi[20]

2.2.1.1. Assumptions. For the present simulations, the left wall has been maintained at a constant temperature T_C (equivalent to the atmospheric temperature of the outer cover) and the right wall has been maintained at a constant temperature T_H (equivalent to steam temperature of the inner cover). Following are the assumptions made in the present work:

(1) The fluid is assumed to be incompressible and Newtonian. Because of the small magnitude of variation in pressure, the density variation is also very small, and hence, the air can be approximated as incompressible. Hence, the flows can be accounted for by only buoyancy variation.
(2) The flow is assumed to be two dimensional.
(3) All the working fluids are operated at temperature differences within the Boussinesq approximation. The well-known Boussinesq equation has been employed, and the density in the buoyancy term is assumed to vary with the temperature according to the following relation

$$\rho = \rho_0(1 - \beta(T - T_0)) \tag{1}$$

$$\text{where, } \beta = \left[\frac{1}{\rho_0}\left(\frac{\partial\rho}{\partial T}\right)\right] \tag{2}$$

(4) Heat transfer by radiation has been neglected, as relatively low temperatures and temperature differences have been considered.
(5) Length (in the third dimension) of the enclosure is sufficiently large so that a two-dimensional motion can be assumed and cylindrical curvature may be neglected.
(6) Variation in properties of air as a function of temperature are assumed to follow the following relations (Incropera and Dewitt[21])

For air

$$\mu = 5\times10^{-8}T + 2\times10^{-6} \tag{3}$$

$$k_t = 8\times10^{-5}T + 0.0016 \tag{4}$$

$$C_p = 0.07T + 985.5 \tag{5}$$

where, temperature T is in Kelvin (K)

2.2.1.2. Governing Equations and Method of Solution. The transient governing equations of continuity, momentum, and energy have been described in Table 1. The term τ_k in Table 1 is transformed as $\tau_k = \mu(\nabla\langle u_k\rangle + (\nabla\langle u_k\rangle)^T)$. The boundary conditions have been described in Table 2. The laminar model equations described in Table 1 have been solved using commercial flow simulation software FLUENT (version 6.2).[22] Transient simulations have been carried out with a time step of 0.0001 s. For each time step, convergence criteria for the sum of normalized residues have been set to 1×10^{-4} for continuity equations, 1×10^{-4} for momentum, and 1×10^{-7} for energy equations. Convergence has been ensured at every time step. The underrelaxation parameters were set to 0.3 for pressure, 1 each for density, energy, and body forces, and 0.7 for momentum equations. In the cited study in ref 4, a segregated solver with implicit time discretization has been employed for obtaining the solution of momentum equations. The momentum equations were discretized using the second-order upwind scheme (SOUS), and for the pressure equation, the PRESTO scheme was used. The SOUS scheme in the commercial software FLUENT 6.2 prevents numerical diffusion while not dampening the disturbances that cause instability. Thus, it ensures spatial accuracy.

2.2.1.3. Grid Sensitivity. The grid test has been performed for aspect ratio ($AR = H_E/L$) of AR = 28 and AR = 174 to ensure grid independent results for the entire AR range. Two *Ra* numbers were chosen for AR = 174 (*Ra* = 907 and *Ra* = 4080) and for

dx.doi.org/10.1021/ie2025745 |*Ind. Eng. Chem. Res.* 2012, 51, 1897–1922

Table 2. Boundary Conditions Used for the 2D Simulation of Air Gap

Boundary Conditions
Initial velocity condition: $u(x,y,0) = v(x,y,0) = 0$ for $0 \le x \le L$ $0 \le y \le H$
Initial Temperature condition: $T(x,y,0) = 0$ for $0 \le x \le L$ $0 \le y \le H$
Initial x-direction boundary conditions: $u(x,0,t) = v(x,0,t) = 0$ for $0 \le x \le L$ and $t \ge 0$
Final x-direction boundary conditions: $u(x,H,t) = v(x,H,t) = 0$ for $0 \le x \le L$ and $t \ge 0$
Final y-direction boundary conditions: $u(0,y,t) = v(0,y,t) = 0$ for $0 \le y \le H$ and $t \ge 0$
Final y-direction boundary conditions: $u(L,y,t) = v(L,y,t) = 0$ for $0 \le y \le H$ and $t \ge 0$
$T_C = 300$, $T_H = 370$ for $0 \le y \le H$ and $t = 0$
$T_C \le T(L,y,t) \le T_H$ for $0 \le y \le H$ and $t \ge 0$
$(\partial T(x,0,t))/(\partial y) = (\partial T(x,H,t))/(\partial y) = 0$ for $0 \le x \le L$ and $t \ge 0$

AR = 28 ($Ra = 2.61 \times 10^5$ and $Ra = 5.81 \times 10^4$). Three different grid distributions were chosen for each AR. For AR = 174, the grids chosen were (A) uniform grid 5 × 870, (B) non-uniform grid 10 × 870 with 75% of the nodes near the walls with the first grid point at $x+ = 0.1$, and (C) non-uniform grid 10 × 870 with 50% of the nodes near the walls with the first grid point at $x+ = 0.1$. Similarly for AR = 28, the same grid distribution was chosen; the numbers being (A) 20 × 560, (B) 40 × 560, and (C) 40 × 560. In all the cases, Case C was found to give the best results, both quantitatively and qualitatively. Hence, the grid distribution of Case C has been selected for all the simulations in the present work.

2.2.2. Results and Discussion. 2.2.2.1. Preamble. This section presents a discussion on the variation in the heat transfer coefficient (HTC) of the insulating air gap (h_{ins}) for a constant ΔT ($\Delta T = 70$ K) by varying the gap width (5 mm ≤ L ≤ 25 mm) and height (H = 560 mm and H_E = 870 mm) of the selected geometry. The term h_{ins} is defined as the time average value of the HTCs from time $t = 0$ to the time when steady state (the convective circulation cell position and number after their formation remains constant and do not affect the HTC, suggesting that the instability has ceased) or quasi-periodic state is reached (cells keep on moving and the number of cells keeps on changing, affecting the HTC, mainly resulting in an increase in magnitude of HTC). Simulations have been performed for the above range (ΔT and AR) and validated with the experimental results. A procedure has then been suggested for estimation of the optimum gap width over typical heating and retention periods (up to 4 h). Using the same procedure, the temperature attained (resultant of supply and losses) after 30 min of heating period for the optimum gap has been predicted, as this is a typical time required for steam cooking of rice and lentils.

2.2.2.2. Effect of Gap Width and Cooker Height on the Heat Transfer Coefficient. Understanding the flow patterns of air inside the air gap is extremely important for the estimation of the net heat flux. Let us consider the maximum temperature at the end of V_{en} to be 373 K (saturated condensing steam at atmospheric pressure), while the minimum temperature at the other end is 303 K (atmospheric room temperature). Thus, the maximum ΔT between inside and outside the ambient temperature is 70 K. The flow patterns at this ΔT have been investigated for different gap widths (5 mm ≤ L ≤ 25 mm) and height (H_E = 560 mm, 870 mm). Figure 2 shows the variation in the insulation

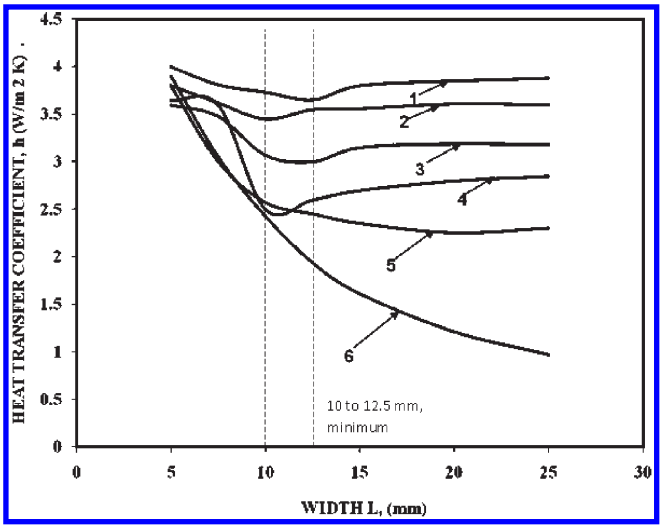

Figure 2. Variation in the insulation heat transfer coefficient (h_{ins}) with gap width (5 mm ≤ L ≤ 25 mm; Δt = 70 K): (1) H_E = 100 mm, (2) H_E = 300 mm, (3) H_E = 500 mm, (4) H_E = 800 mm, (5) H_E = 1000 mm, (6) heat losses by only conduction.

heat transfer coefficient (h_{ins}) with gap width (5 mm ≤ L ≤ 25 mm; ΔT = 70 K). Line 6 is drawn to show the quantum of heat loss by conduction only with a stagnant air gap. This line (locus of values of all h_{ins} values representing pure conduction) is independent of the height of the air gap because no air currents are assumed in pure conduction. The remaining lines in Figure 2 represent the variation in h_{ins} with gap width for different heights. It should be noted that the h_{ins} values remain constant after a certain gap width for any specified height over the entire range (500 mm ≤ H_E ≤ 1000 mm) considered in this work, and the observed constant value of h_{ins} is higher for lower heights. It is expected that as gap width increases, insulation capability increases (provided the air is stagnant), and hence, the h_{ins} should decrease. However, it has been observed that after a certain width there is no decrease in h_{ins}, and the h_{ins} becomes independent of the gap width and then remains practically constant. This is explained as follows. As the gap width increases [Figure 3; H_E = 560 mm, 870 mm; L = 15 mm (refer lines 2 and 3)], the local HTCs are enhanced due to flow fluctuations arising out of natural convection (formation of the multiple circulation cells in the central part of the air gap).[4] Hence, when the height is low, the h_{ins} is high. Further, as height increases, the magnitude of HTCs at the top and bottom increases, but the h_{ins} remains constant. This can also be explained in terms of flow patterns as represented in Figure 3, which shows flow patterns for different gap widths (5 mm ≤ L ≤ 20 mm; ΔT = 70 K; H_E = 560 mm; 870 mm) Panel (A i, ii) of Figure 4 (L = 5 mm, 8 mm) and panel (B vii, viii, ix) of Figure 4 (L = 5 mm, 8 mm, 10 mm) show unicellular patterns which represents that conduction is the main mode of heat transfer, while panel (A iii, iv, v, vi) of Figure 4 and panel (B vii, viii, ix, x, xi, xii) of Figure 4 represent multicellular patterns and a significant contribution of natural thermal convection to the overall heat transfer. For a height H_E = 500 mm, multicellular cells start forming at L = 10 mm and above, while for H_E = 1000 mm, they start at L = 12.5 mm and above. However, Figure 2 shows that minimum h_{ins} occurs at L = 12.5 mm (line 4, Figure 2, band of 10−12.5 mm). This is due to the contribution of heat transfer coefficients at the top and bottom of the air-gap

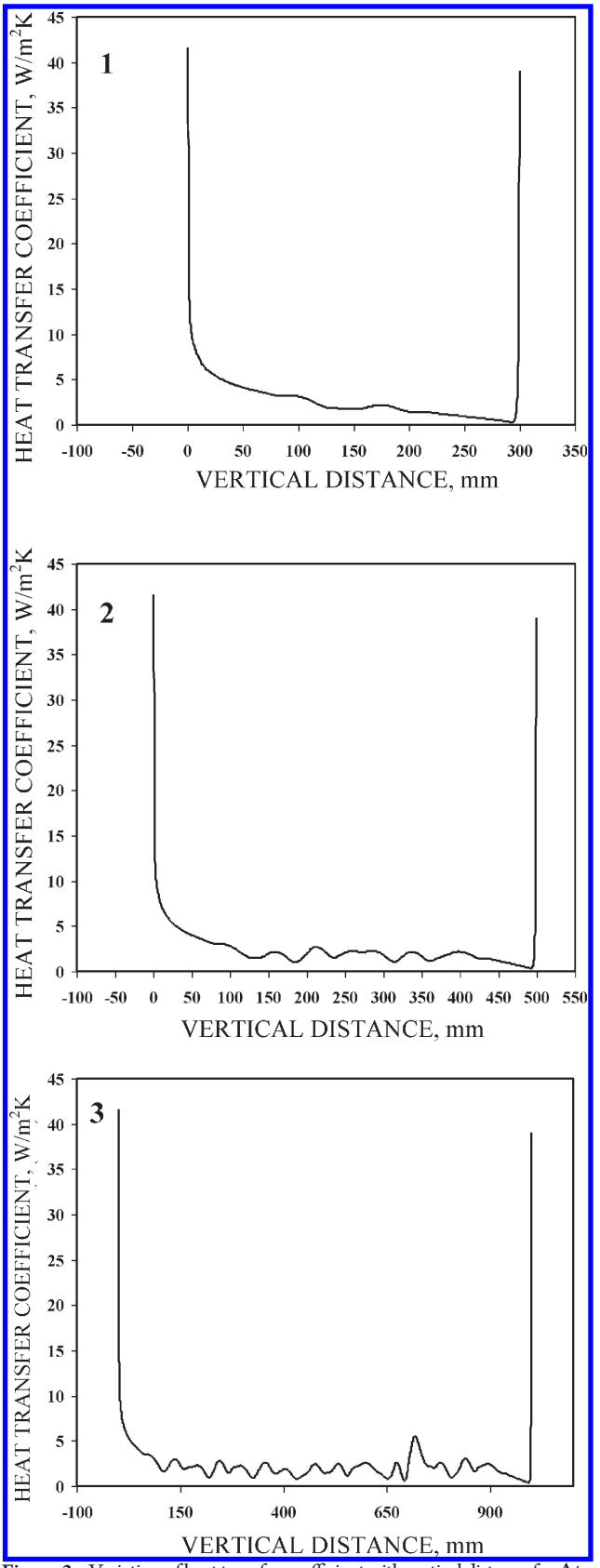

Figure 3. Variation of heat transfer coefficient with vertical distance for Δt = 70 K and L = 15 mm: (1) H_E = 300 m, (2) H_E = 560 mm, (3) H_E = 870 mm.

as shown in Figure 2. The fluid mixing at the top and bottom part of the air gap is lower in the case of a gap of 12.5 mm than that for other gap widths, giving h_{ins} for L = 12.5 mm to be the lowest.

2.3. Heat Transfer from Steam to Water. *2.3.1. Preamble.* A schematic diagram of pots in the cooker is shown in Figure 1. The contents of the pots are heated by condensation of steam on the outer surface of the cylinder. Steam is also condensed on the bottom surface of the pot if suitable spacing is maintained between pots. The transfer of heat from water results in natural convection in the pool of water inside the pot. When the water contains rice/lentils/vegetables, these immersed bodies provide resistance to natural convection. It was thought desirable to undertake CFD simulations of the heat transfer process so that the optimum selection for the following are possible. Initially, transfer of heat from condensing steam to water (single phase) has been considered.[4] The modifications in the flow pattern in the presence of immersed particles can be estimated using the procedure of Reddy and Joshi[5] (Section 2.4). The following stepwise procedure was employed:

(a) The estimation of the heat transfer rate for all the pots gives the qualitative number for the rate of heat supply by the burning of LPG. This exercise needs to be carried out at various stages of cooking.

(b) The possibility of stratification is known to occur in the process of heat transfer. Further, the food does not get cooked in the low-temperature stratified region. This feature puts a limit on the pot size and the aspect ratio.

(c) As mentioned previously, natural convection gets dampened by the presence of rise/lentils/vegetables in the pool of water. Therefore, it is desirable to understand the stratification and heat transfer in the presence of these materials.

(d) The stratification can be lessened by providing suitable internals in the pot. The modified geometries permit pressure and flow redistribution.

It was thought desirable to address all of the above issues using CFD simulations. For this purpose, three-dimensional simulations were employed against two-dimensional simulations of the air gap in Figure 1. One-quarter of the pot was considered for the modeling and is shown in Figure 4 together with the coordinate system and grids.

2.3.2. Previous Work. Ganguli et al.[4] and Gandhi et al.[23] have comprehensively reviewed the literature. The following is a brief summary:

Aszodi et al.[24] measured the temperature field in their system with thermocouples and simulated the same using commercial software CFX4, using the wall-boiling model included therein. It was assumed that neither temperature nor gas fraction influences the density of the liquid and that the momentum of the gas phase was negligible. These assumptions are rather restrictive.[20]

Kang[25] has experimentally investigated the thermal mixing in a rectangular water tank being heated by steam. He has reported the effect of tube orientation (i.e., horizontal or vertical) on natural convection. He has concluded that the time required for achieving the saturation temperature of water is independent of the tube orientation.

Krepper et al.[26] have investigated natural convection in a large pool using temperature measurements and CFD simulations using commercial code CFX-4. They have used a laminar flow model for the system to investigate temperature oscillations due to presence of a plume near the tube surface.

Calcagni et al.[27] have carried out experimental (thermocouples for temperature measurements and holographic interferometer

for flow measurements) and numerical analysis of air in a square enclosure approximating a two-dimensional vertical slot. The air was partially heated by a centrally located heating element from the bottom, with the vertical walls acting as cooling elements. The other surfaces were considered adiabatic. The numerical simulations were performed using the commercial code FLUENT 6 assuming two-dimensional geometry. They have concluded that in a vertical slot, Rayleigh number (Ra) less than 10^4, heat transfer takes place mainly by conduction, while for Ra equal to 10^5, heat transfer takes place by convection.

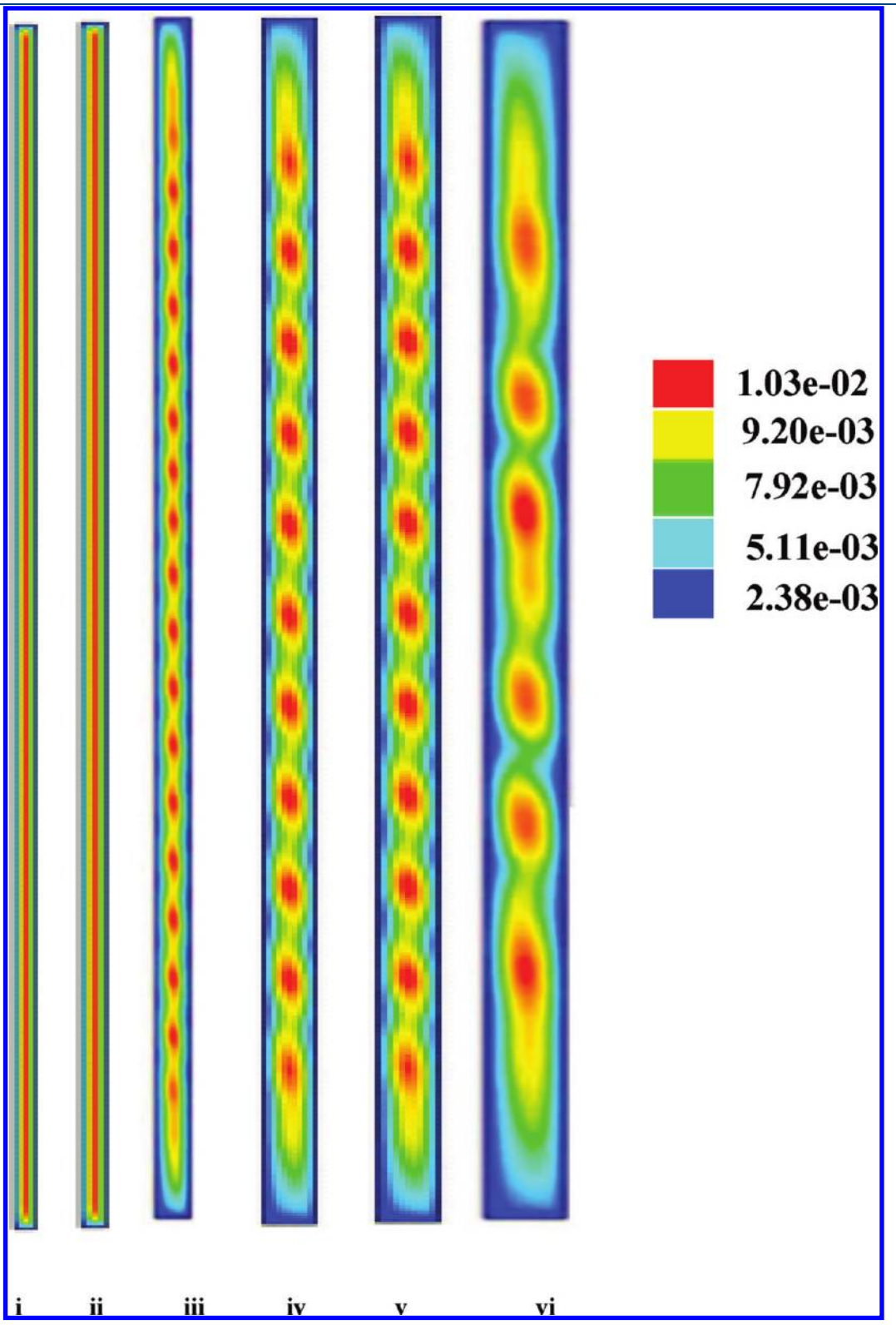

Figure 4. Continued

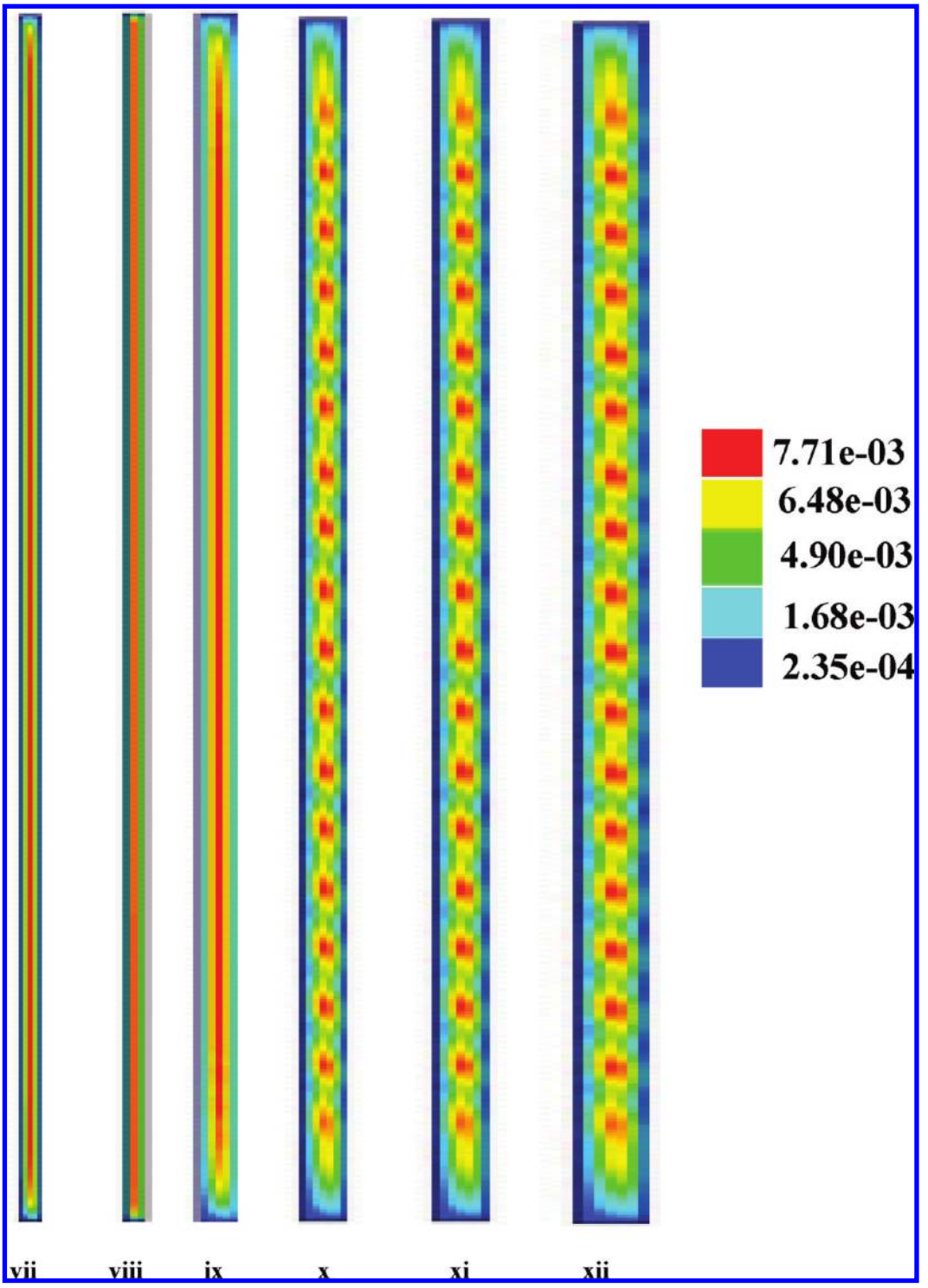

Figure 4. Flow patterns for various gap widths for $\Delta t = 70$ K. (A) $H_E = 560$ mm, (i) $L = 5$ mm, (ii) $L = 8$ mm, (iii) $L = 10$ mm, (iv) $L = 12.5$ mm, (v) $L = 15$ mm, (vi) $L = 20$ mm. (B) $H_E = 870$ mm, (vii) $L = 5$ mm, (viii) $L = 8$ mm, (xi) $L = 10$ mm, (x) $L = 12.5$ mm, (xi) $L = 15$ mm, (xii) $L = 20$ mm.

Sharma et al.[28] have investigated turbulent natural convection in a rectangular enclosure heated from the bottom using numerical simulations of a two-dimensional geometry using commercial codes (FLUENT, PHONIX, STAR-CD) as well as an in-house code. They have considered air as the working fluid with *Ra* ranging from 10^8 to 10^{12}. They have investigated the effect of different boundary conditions (constant temperature, constant heat flux) on natural convection by performing steady state as well as transient simulations. They have reported two counter-rotating cells for the entire range of *Ra* numbers and for various values of heated width and have found that for isothermal heating, the Nusselt number (*Nu*) increases with an increase in

dx.doi.org/10.1021/ie2025745 |*Ind. Eng. Chem. Res.* 2012, 51, 1897–1922

the heated width. The opposite was found to be true for isoflux heating. They have concluded that the Nusselt number is a weaker function of heated width for isoflux heating compared to isothermal heating. They also concluded that the intensity of buoyancy-induced flow in the case of isoflux heating is lower compared to that from isothermal heating at identical values of *Ra*. They have proposed correlations for the Nusselt number (*Nu*) for both boundary conditions.

Ganguli et al.[4] have performed CFD simulations and experimental measurements for a centrally heated tube placed in a cylindrical enclosure. They have measured the flow patterns by PIV measurements and hot film anemometry (HFA). Temperature patterns were obtained using thermocouples. They have performed CFD simulations for a two-dimensional axi-symmetric geometry using commercial software FLUENT 6.3 with a user-defined function (UDF) for incorporation of their phase change (boiling) model. The value of *Ra* was varied in the range from 4.98×10^{12} to 3.764×10^{13}. They have considered water as a working fluid, and density variation has been modeled using the Boussinesq approximation.

2.3.3. Numerical Procedure. 2.3.3.1. Governing Equations. In order to model unsteady natural convection with possible stratification, the governing equations (continuity, momentum, and energy) with the appropriate Reynolds stress closure need be solved. In the present work, a shear stress transport (SST) k-ω turbulence model has been used. All the equations for single-phase simulations (only natural convection) are listed in Table 1. For solving the equations, open source CFD software OpenFOAM-1.6 was used. In the present case, the following assumptions have been made to model the heat transfer.

2.3.3.2. Model Assumptions

(1) Condensation occurring outside the wall is film condensation, and hence, the wall is at a constant temperature.
(2) Outside heat transfer coefficient varies along the length or height of the wall.
(3) Fluid is Newtonian in rheological behavior and is incompressible.
(4) The Boussinesq approximation is valid, i.e., density differences are only important in producing buoyancy.
(5) There are constant fluid properties (such as viscosity), except in the formulation of the buoyancy term.

2.3.3.3. Grid Independence. In the present work, a cylindrical pot has been considered, and only a quarter of the geometry (Figure 5) has been used for grid generation. Therefore, the total computational time is reduced. Grid independence was investigated by considering three different grid cases: (a) 450,000; (b) 750,000, and (c) 850,000. A non-uniform hexahedral grid was used with a finer grid near the tube wall where gradients are more important compared to zones away from the tube wall. Approximately 70% of the nodes were located in the boundary layer, and 30% were located in the core region where (according to the experimental results) the fluid is essentially quiescent and the temperature varies linearly along the length of the pot wall. It was ensured that at least one should be in the viscous sublayer ($y^+ < 5$) and several nodes in the buffer and turbulent zones. For these three cases, we have compared the results of mean quantities at different positions. All the chosen grids predict mean flow patterns effectively, but for further simulations a grid size of 750,000 cells has been used. Minor differences have been observed between 750,000 and 850,000. However, these were found to be within the ±5% average error.

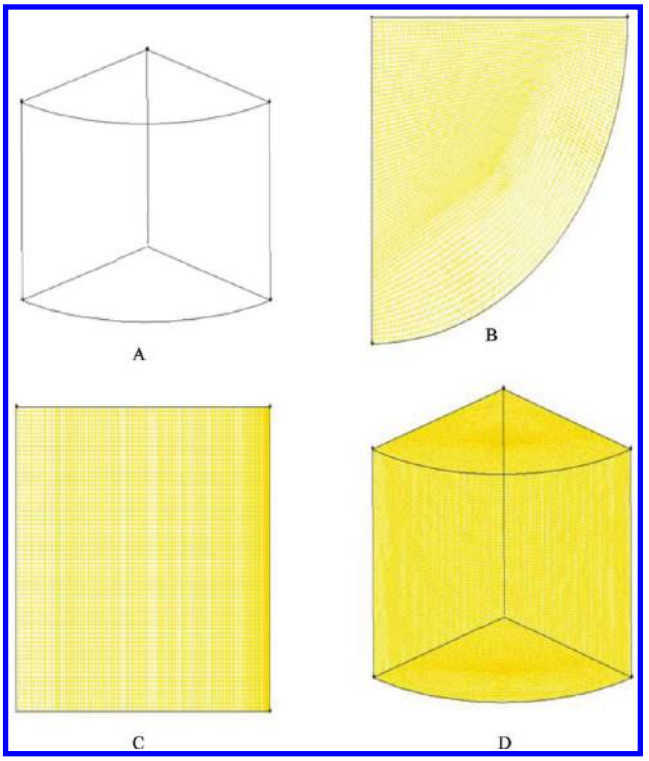

Figure 5. Geometry used for simulation along with coordinate system and grid size: (A) geometry used, (B) top view, (C) side view, (D) geometry showing meshing details.

2.3.3.4. Boundary Conditions. The bottom wall of the tank was considered with no slip boundary condition. Further, two cases of thermal conditions were considered for the bottom wall: (i) adiabatic and (ii) heat transfer from condensing steam. Free slip and adiabatic boundary conditions were employed for the top water surface. A constant temperature boundary condition has been given to the wall together with no slip. These details are listed in Table 2.

2.3.3.5. Method of Solution. All of the computational work has been carried out using the open source software OpenFOAM- 1.6 with the buoyant BoussinesqPisoFOAM solver. The second order implicit scheme has been used for time discretization. In the case of the k-ω model, the QUICK discretization scheme was used for turbulence parameters. For the final sweep over each segment, upwinding has been performed using QUICK with a second-order pressure scheme. The QUICK formulation has a third-order accuracy that helps to mitigate the unfavorable effect of artificial diffusion that can occur when using low-order upwinding schemes. All the solutions were considered to be fully converged when the sum of residuals was below 10^{-5}. All the computations have been performed on an SGI cluster with quad processor nodes with a 2 GB RAM, 2.4 GHz processor speed.

2.3.4. Heating of Single Pot. For the initial transient period (t = 30s), we see a strong temperature gradient near the vicinity of the wall and practically no gradient in the middle of the enclosure. Thus, the water near the wall gets heated and rises. Water from the neighboring areas rushes to take the place of the risen water and motion of water starts in the pot. Figure 6 shows a schematic representation of the velocity variation with dimensionless lateral distance. We observe that there is a velocity

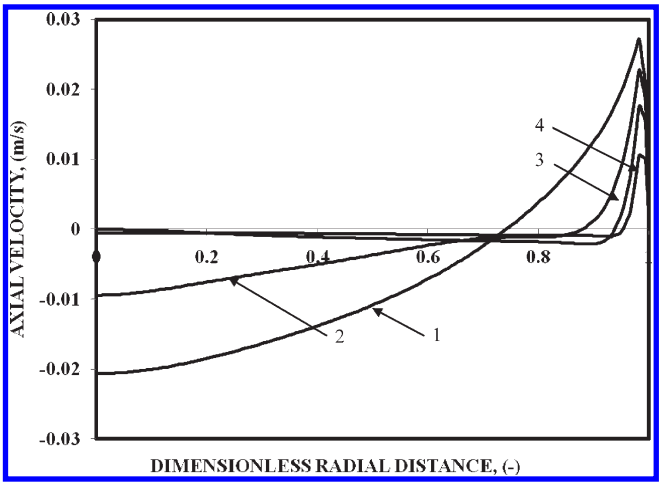

Figure 6. Schematic representation of the axial velocity variation with dimensionless lateral distance: (1) t = 30 s, (2) t = 100 s, (3) t = 200 s, (4) t = 500 s.

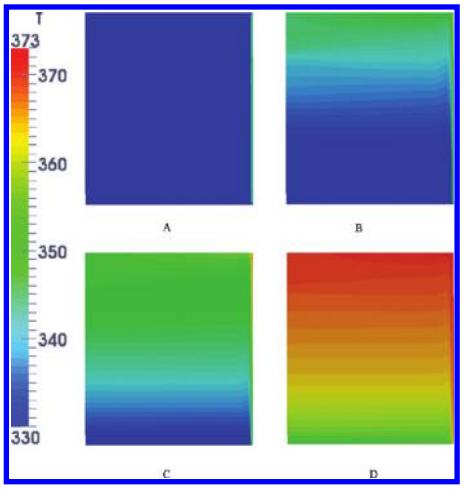

Figure 7. Temperature contours at different times: (A) t = 50 s, (B) t = 150 s, (C) t = 250 s, (D) t = 350 s.

peak near the wall, and the velocity decreases as we move away from the wall. In the middle region, velocity becomes zero, and values becomes negative as we move toward the center of the pot. Negative velocity implies the downward flow of water in the central region. This shows that the material balance in the tank is maintained at every point in time. Eventually, the boundary layer flow adjacent to the wall begins. As time passes, hot water starts accumulating at the top water surface because it is lighter than the water in the middle region of the tank.

Figures 7 and 8 show schematic representations of snapshots of the temperature isotherms and flow pattern. It is observed that the extent of stratification increases as time progresses. In particular, the size of the dead zone increases with time.

2.3.5. Extent of Stratification. The stratification parameter has been proposed and defined by Han et al.[29] It is defined as the ratio of the mean temperature gradient at any time to the maximum mean temperature gradient achieved at the end of the run. The stratification number varies from zero to one, with zero representing no stratification (complete mixing) and one representing

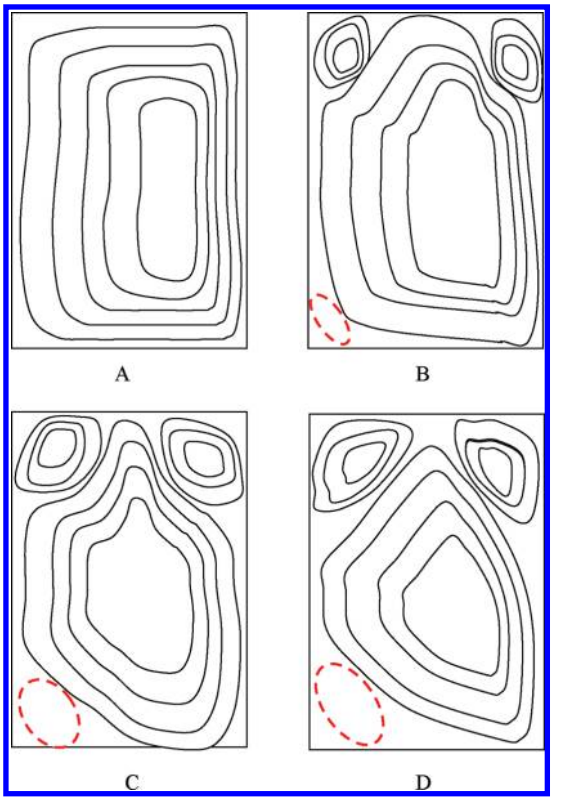

Figure 8. Streamline plots at different times: (A) t = 50 s, (B) t = 150 s, (C) t = 250 s, (D) t = 350 s.

maximum stratification. Mathematically, stratification at any time can be expressed as

$$S = \frac{\langle(\partial T/\partial y)\rangle}{(\partial T/\partial y)_{max}} \tag{6}$$

where

$$\left\langle\left(\frac{\Delta T}{\Delta y}\right)\right\rangle = \frac{1}{j-1}\left[\sum_{j=1}^{j-1}\left(\frac{T_{j+1}-T_j}{\Delta y}\right)\right] \tag{7}$$

$$\left\langle\frac{\Delta T}{\Delta y}\right\rangle_{max} = \frac{T_{max}-T_{min}}{(j-1)\Delta y} \tag{8}$$

In simulations and experimental measurements, temperatures have been monitored at different axial locations, and the values of $(\Delta T/\Delta y)$ and $(\Delta T/\Delta y)_{max}$ have been calculated by eqs 7 and 8. Runs have been carried out for a time of 1200 s. In both cases, the data have been analyzed using the same procedure. It was observed that at any particular time instant the stratification number was found to increase with an increase in the *Ra* number. Thus, systems with a higher *Ra* number get stratified faster compared to those at a lower *Ra* number. Indirectly, sizes of all dead zones increase with an increase in pot size.

2.4. Heat Transfer from Steam to Water−Rice (Solid Particles) Mixture at Various Stages of Cooking. *2.4.1. Preamble and Previous Work.* In Section 2.3, we analyzed the problem of heat transfer from steam to water. In this case, the steam condenses on the outside wall of the pot, and the water in the pot is heated from room temperature to the desired temperature.

dx.doi.org/10.1021/ie2025745 |*Ind. Eng. Chem. Res.* 2012, 51, 1897–1922

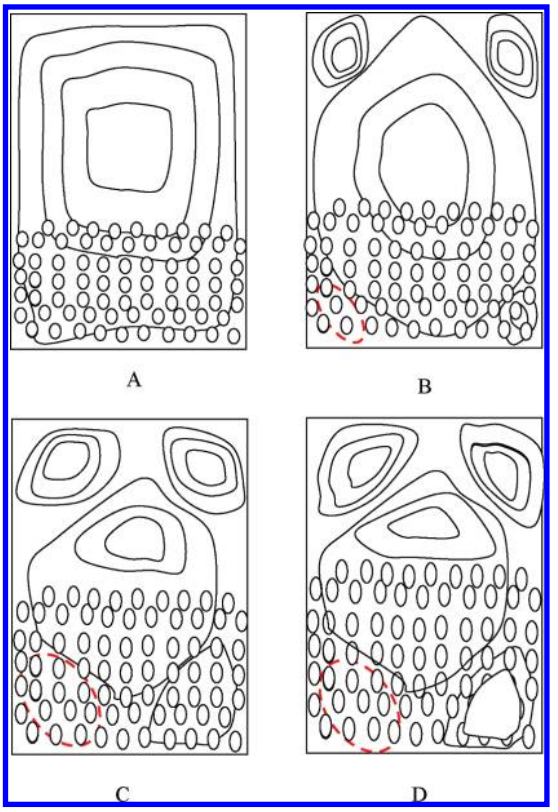

Figure 9. Streamline plots at different times in the presence of solid particles: (A) t = 50 s, (B) t = 150 s, (C) t = 250 s, (D) t = 350 s.

When the material to be cooked is added to water in the required proportions (for instance rice to water, 1:2, and lentils to water, 1:3), the solid phase forms a fixed bed at the bottom. The solid phase can be rice, lentils, potatoes, or vegetables. In other words, at the beginning of cooking, the solid phase can have different particle sizes, particle size distribution, and voidage. During cooking, all the material swells, and the voidage (volume fraction of free flowable water) changes according to the stage of cooking. Thus, the height of the fixed bed also changes with respect to cooking time. Water is present above the fixed bed and also in the interstices of the fixed bed.

Thus, in the present case, heat transfer occurs from steam to a fixed bed in the bottom region and steam to water in the top region of the pot. The latter problem was addressed in Section 2.3. Now, let us consider the problem of heat transfer from steam to fixed bed.

2.4.2. CFD Simulation. Reddy and Joshi[5,30] have performed CFD simulations of the flow pattern in a fixed bed. The authors have given details pertaining to the CFD simulations consisting of governing equations, boundary conditions, numerical procedure, grid size effect, etc. The results of these studies were used to understand the convective flow pattern of the water in a cooking pot.

2.4.3. Result and Discussion. As said previously, the cooking pot consists of a fixed bed at the bottom and free water at the top. The solid particles provide resistance to flow, and the flow patterns as shown in Figure 8 are modified. These are shown schematically in Figure 9. It may be pointed out that the height of the fixed bed increases with respect to time in the cooking process. The value of the convective fluid velocity decreases in the presence of the fixed bed. The size of the dead zone also increases. In particular, the size

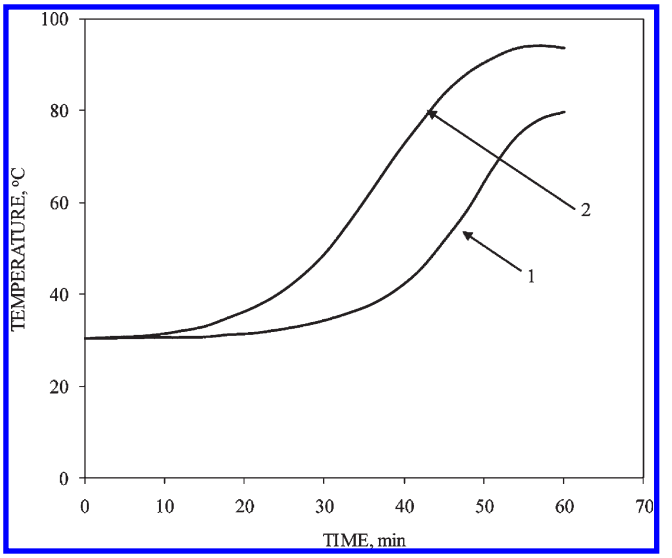

Figure 10. Temperature variation at two different axial locations: (1) near bottom, (2) near top.

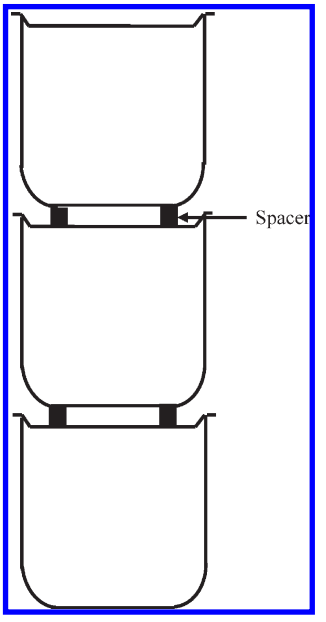

Figure 11. Modified arrangement of pots/vessels; spacers placed in between pots/vessels.

of the dead zone in the central bottom region increases. Because this region is away from the location of condensing steam, the rate of the rise of temperature was found to be relatively slow and did not even reach the cooking temperature as shown in Figure 10 at this location. In fact, rice was found to be uncooked in this region. The intensity of the problem obviously increases with an increase in pot size and depends as well on the type of food and the water quantity.

We need to ensure complete cooking in all parts of the pot in as short a time as possible. For this objective, the dead zone in the central bottom region needs to be eliminated or at least some fluid convection needs to occur. For this purpose, two modifications have been employed.

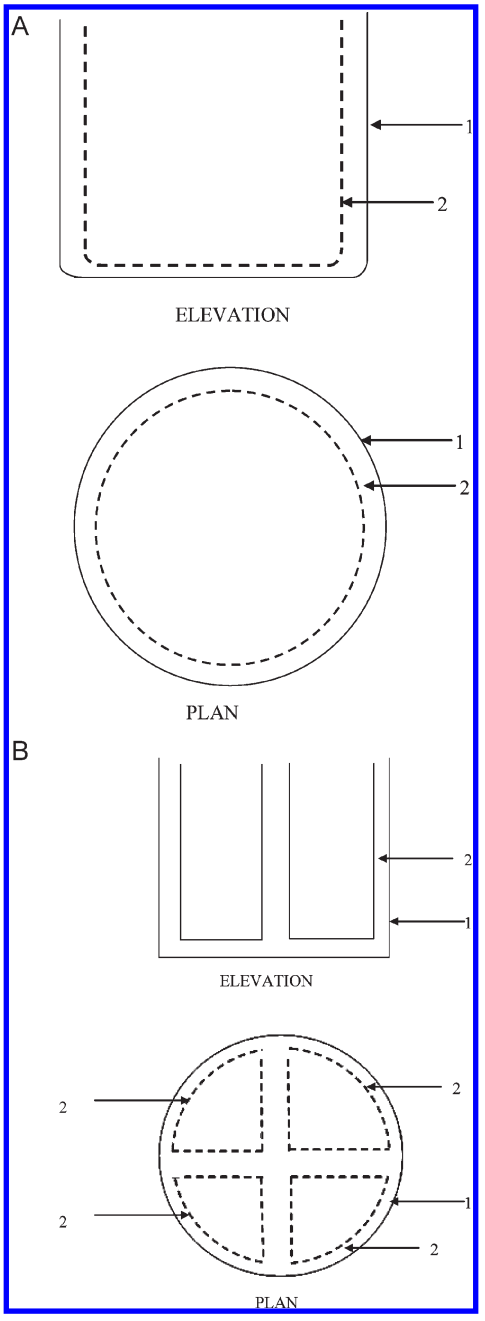

Figure 12. Pot with different internals: (A) smaller pot with perforations, (B) four perforated quarter parts, (1) vessel, (2) perforated vessel of quarter vessel.

In the first modification, spacers were placed between the pots (Figure 11). As a consequence, steam was allowed to enter and condense on the bottom outer side of the second and third pots. This modification increases the total heat transfer area (which otherwise is not easily modifiable) and also puts the enthalpy source near the observed dead zones and uncooked material location. This modification reduces the size of dead zone. For further reduction in size of dead zones, two types of internals were attempted:

(1) Another perforated pot (2 in Figure 12 A) was placed inside the original pot (1 in Figure 12 A) with a gap of about 5 mm all round as well as on the bottom (Figure 12A). Food items were kept inside the perforated pot. Water could remain present in the outside gap as well as in the perforated pot. Temperature profiles measured at the same locations (as shown in Figure 10) are shown in panel (A) of Figure 13. Substantial influence can be seen on the dead zone, where the temperature profile is observed to reach the cooking temperature and also in a shorter time (Figure 13A).

(2) In the second modification, four quadrant-shaped perforated pots (2 in Figure 12 A,B) were kept inside the original pot with gaps on the side (2 in Figure 12 B), middle, and bottom (Figure 12B). The temperature profiles in panel (B) of Figure 13 are also shown to reduce the presence of dead zones, resulting in a faster temperature rise.

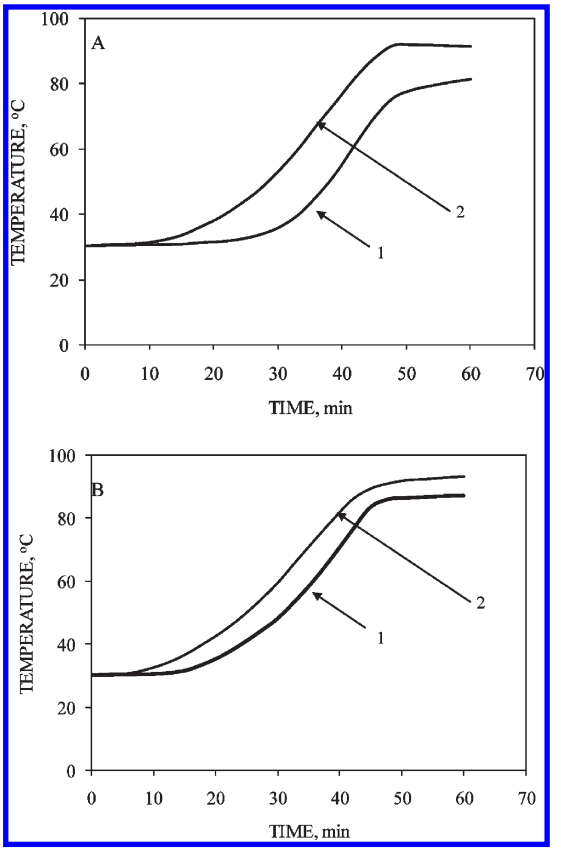

Figure 13. Temperature variation at two different axial locations along with internals: (A) smaller pot with perforations, (B) four perforated quarter parts, (1) near bottom, (2) near top.

Either of the two modifications permitted an increase of pot size from 280 mm to 510 mm. Even larger sizes are yet to be examined and may allow an even higher initial charge of rice and water.

3. COOKING OPTIMIZATION

The systematic development of a cooker was described in Part I. Sections 4, 5, and 6 have described the development of the cooker with optimization of energy efficiency. In all the earlier cases, only water was used as the charge. It was thought desirable to evaluate the performance of the cooker developed earlier for cooking of rice and lentils and, if necessary, optimize the design further.

dx.doi.org/10.1021/ie2025745 |*Ind. Eng. Chem. Res.* 2012, 51, 1897–1922

Table 3A. Gas Consumption To Cook 100 g Rice in Cooker of Different Capacities

S.N.	cooker capacity (L)	charge		LPG flow rate (mL/s)	time (s)	total G.C. (g)	gas consumption per 100 g food item (g)
		rice (kg)	water (liter)				
1	4.5	1.5	3.0	6.6	4220	64	4.3
2	6.0	2.0	4.0	7.3	4880	82	4.2
3	24.0	8.0	16.0	27.6	5200	330	4.1
4	72.0	12.0	24.0	83.3	2580	495	4.1
5	72.0	16.0	32.0	84.2	3340	646	4.0
6	72.0	20.0	40.0	84.8	4090	798	4.0
7	72.0	24.0	48.0	85.8	4820	950	3.95

Table 3B. Gas Consumption To Cook 100 g Lentils in Cooker of Different Capacities

S.N.	cooker capacity (L)	charge		LPG flow rate (mL/s)	time (s)	total G.C. (g)	gas consumption per 100 g food item (g)
		lentils (kg)	water (L)				
1	4.5	1.1	3.3	6.6	4350	66	6.0
2	6.0	1.5	4.5	7.3	5120	86	5.7
3	24.0	6.0	18.0	27.6	5370	341	5.7
4	72.0	9.0	27.0	83.8	2620	505	5.6
5	72.0	12.0	36.0	84.8	3380	660	5.5
6	72.0	15.0	45.0	84.1	4270	826	5.5
7	72.0	18.0	54.0	86.9	4850	970	5.4

3.1. Cooking Performance of Cooker. A new set of cooking experiments were performed with "Surti Kolam" variety of rice in the proportion of 1:2 with water. Cookers of 4.5, 6, and 24 L were charged to the full capacity, and the cooker of 72 L capacity was charged to 50%, 67%, 83%, and 100% capacity as described in Section 6. Thermocouples were inserted in all the vessels and the water in the base. Gas was supplied at respective flow rates (similar to those employed for the heating profile) until the charge temperature reaches 98 °C. Retention was then allowed for 30 min, after which the cooker was opened. Rice grains in all the vessels were tested for the extent of cooking. It was observed that the grains were satisfactorily cooked to the required texture. Similar experiments were performed for "Arhar (Tuvar)" variety of lentil (dal) in 1:3 proportion with the water. Lentils also were observed to be nicely cooked and could be mashed easily. Gas consumption figures for cooking of unit quantities of 100 g rice and 100 g lentils are listed in Tables 3A and 3B, respectively. From the knowledge that the rice grain cooking starts at 74 °C onward (depending on the quality of rice) and lentil grain cooking starts at 94 °C (which also depends upon the quality of lentils), it can be observed that the gas consumption in the case of rice is less than that for lentils at their respective optimum ratios with water. It has also been observed that the gas consumption per unit quantity of food item reduces as cooker capacity increases. It may be pointed out that the pressure cookers are hardly available beyond 30 L capacity of the outer vessel.

3.2. Standardization and Optimization of Parameters for Cooker. In order to examine the performance of the present cooker, a 72 L capacity model was supplied in December 2002 to the Post Graduate (PG) Students Mess at the Institute of Chemical Technology (ICT), Matunga, Mumbai, India, that caters to 300 students at a time. Its regular requirement of food items at a time using the usual cooking method is 14 kg of rice and 4.5 kg of lentils (tuvar). Potato requirement is about 6 kg . Using the traditional method of cooking for rice, lentils, and potatoes, the mess earlier required about 14 LPG cylinders of 14.2 kg net weight per month. Prior to the introduction of the new cooker, the food items were cooked by conventional methods (open pan cooking). For instance, lentils and potatoes were cooked by boiling. Rice was cooked by the "drain method" that is a common practice whenever rice has to be cooked on a large scale. After the introduction of a new cooker, the LPG cylinder requirement was found to be reduced from 14 to 6.

3.2.1. Experimental Setup and Procedure. Three types of burners, namely, torch, sunbeam, and moonbeam, have been examined (BIS standard[31]). The base of the 72 L model of the cooker was placed on the LPG burner. The required quantity of water was poured in the base. Three stands (for vessel stacks) were placed in the base. The vessels with requisite quantities of charge were placed in the stands. Thermocouple probes were inserted in water in the base and in the pots. Inverted plates were kept on top of vessels (V_4) in all three stacks. Wire stands were provided to avoid the movement of vessels within each stack. The LPG regulator was switched on, and the flow control valve was adjusted in such a manner that the flame diameter was about one-third of the base diameter. The cooker contents were heated until they reached boiling point at which point the gas supply was switched off. Retention was then allowed, without opening the cooker. Gas flow rates during heating and temperatures of the various components during heating and retention were measured at predetermined time intervals.

3.2.2. Water in Base. The condition required during the cooking operation was that the water in the base should touch the bottom pots (V_1) during the heating period, whereas the contact between water and vessel V_1 should be broken during retention. In order to optimize the water quantity in the base, cooking experiments were carried out by keeping lentils in bottom vessels (V_1) and rice in the upper pots (V_2, V_3 and V_4).

Table 4A. Optimum Water Quantity for Cooking of Rice in Metal Covered Vessel[a]

				water losses (g)		
water quantity (g)	gas flow rate (mL/s)	time required (s)	gas consumed (g)	heating	cooling	result
200	4.3	1110	11	20	62	undercooked
	7.3	800	13.5	20	65	undercooked
	21.4	420		burnt without cooking		
300	4.3	1210	12	22	75	cooked
	7.3	890	15	22	80	undercooked
	21.4	470		burnt without cooking		
400	4.3	1320	13	21	70	cooked
	7.3	980	16.5	23	84	cooked
	21.4	510		burnt without cooking		
500	4.3	1470	14.5	22	74	cooked
	7.3	1070	18	24	88	cooked
	21.4	610	30	26	233	cooked

[a] Rice quantity = 100 g, Vessel capacity = 5.0 L, D = 180 mm, H = 220 mm.

Table 4B. Optimum Water Quantity for Cooking of Lentils in Metal Covered Vessel[a]

				water losses (g)		
water Quantity (g)	gas flow rate (mL/s)	time required (s)	gas consumed (g)	heating	cooling	result
200	4.3	1420	14	45	118	Undercooked
	7.3	950	16	48	120	undercooked
	21.4	780		burnt without cooking		
300	4.3	1620	16	51	119	cooked
	7.3	1070	18	52	123	cooked
	21.4	810		burnt without cooking		
400	4.3	1720	17	52	124	cooked
	7.3	1190	20	59	133	cooked
	21.4	860		burnt without cooking		
600	4.3	2120	21	60	142	cooked
	7.3	1370	23	61	147	cooked
	21.4	950		burnt without cooking		
800	4.3	2530	25	61	166	cooked
	7.3	1550	26	64	202	cooked
	21.4	1040	51	75	382	cooked

[a] Lentils quantity = 100 g, vessel capacity = 5.0 L, D = 180 mm, H = 220 mm.

During heating and retention, temperatures of charge in all the pots were also noted.

During the experimentation, it was observed that for 10 L quantity of water in the base, rice in all the pots was nicely cooked. Lentils in two pots (bottom pots of two stacks) was undercooked. Pots containing lentil that was undercooked showed final temperatures of 84 and 88 °C. It indicates that these pots were not in contact with the water in the base for a sufficient time, resulting in their inadequate heating. Hence, the water quantity in the base was increased to 12 L, keeping other conditions the same. It was observed that the rice in all the vessels was nicely cooked, but the lentils in one vessel was undercooked. The temperature of the charge in this vessel was 91 °C. The water quantity in the base was further increased to 15 L, and cooking was carried out. It was observed that rice in all the vessels was nicely cooked. However, lentils in all three vessels was undercooked, despite the temperatures of charges in these vessels having reached 98 °C. This was because the temperature in those vessels dropped considerably during the retention period resulting in undercooking. This indicates that the cooking pattern in the bottom pots is governed by three parameters: (1) Quantity of water in the base should be sufficient so that it is in continuously in contact with the bottom vessels during heating. (2) There should be no contact between the two during the retention time. (3) The base should be perfectly horizontal if we want to use minimum water quantity in the base (any inclination may result in different extent of contacts for different vessels).

From Section 4.6 of Part I, it can be observed that for the water quantity of 12 L in the base, food items in all the pots were nicely cooked. Comparing these results with the present one, it can be concluded that the discrepancy in cooking of the charge in the bottom pots was because of the base that was not in a perfectly horizontal position. Even in actual field practice, it may not be possible, willingly or unwillingly, to keep it in a perfectly horizontal

position because of the relatively large size of the base. Hence, a drain tap was provided in the base in order to drain excess water at the commencement of the retention period.

Drain tap has a position in the base such that even if it is kept open about 7 L of water is retained in the base. At this condition, water in the base does not touch the bottom pots (V_1). Fifteen liters of water was sufficient to maintain contact with the bottom pots, even if the base is in a slightly tilted position. At the start of retention, excess water can be drained by opening the tap.

3.2.3. Gap between Pots. In this cooker, heat is transferred to the contents of the vessel via condensation of steam on the outside surface of vessel. Thus, the arrangement of vessels V_1, V_2, and V_3 plays a vital role in the cooking operation. The arrangement of vessel decides the actual area available for steam to condense and thus the rate at which heat energy is transferred to the contents of vessels. Stacking of vessels one over another (Figure 1) blocks the bottom area of vessels V_2 and V_3. Contents of vessel V_1 is heated at much faster rate compared to vessels V_2 and V_3, as V_1 is always in physical contact with boiling water. Then the content of the top vessel V_3 is heated and finally the middle vessel V_2. This difference in the rate of heating for vessels V_2 and V_3 sometimes results in a difference in the quality of cooked food.

This difference in heating rate is eliminated by simply adding spacers between vessels (Figure 11). This arrangement ensures that the area available for steam to condense in vessels V_2 and V_3 remains same. A uniform rate of heating is achieved by this arrangement for vessels V_2 and V_3, and thus the quality of cooked food in those vessels is uniform as well.

3.2.4. Water Ratio on Smaller Scale. Different food items require water in different proportions for cooking. To see the effect of water proportion on cooking characteristics, experiments were performed with different ratios, and these are described in the following sections.

In order to investigate the effect of the quantity of water, different quantities were added to 100 g of rice or lentils. Experiments were performed at gas flow rates of 4.3, 7.3, and 21.4 mL/s using the 5 L vessel (D = 180 mm, H_E = 220 mm) with lid and insulating metal covers. The results based on the required texture and consistency of the cooked material are listed in Table 4A for rice and in Table 4B for dal (lentils).

The following observations were made: (a) When it was observed that a food item gets stuck to the vessel base that is in direct contact with the flame during heating, further heating was stopped as it would result in burning of the food item. This was the case when the water quantity added to the food item was completely evaporated before completion of the cooking process. This could be guessed easily for smaller flow rates, at which time the gas supply was stopped. It was considered as the primary stage of food burning. However, for the higher flow rate, 21.4 mL/s, early detection of primary burning was found difficult, and the food item was almost burnt without cooking. (b) For a rice to water ratio of 1:3, rice was cooked at the LPG flow rate of 4.3 mL/s, partially undercooked for the flow rate of 7.3 mL/s, and burnt without cooking for the flow rate of 21.4 mL/s. However, it remained undercooked for these flow rates for the 1:2 ratio. Hence, the optimum ratio at lower flow rates is 1:3. At a higher flow rate of 21.4 mL/s, the optimum ratio is 1:5. (c) For a lentils to water ratio of 1:3, lentils were cooked at a LPG flow rate of 4.3 mL/s, partially undercooked for a flow rate of 7.3 mL/s, and burnt without cooking for a flow rate of 21.4 mL/s. However, it remained undercooked for lower flow rates for 1:2 ratio. Hence, the optimum ratio can be considered as 1:3. At a higher LPG flow rate of 21.4 mL/s, the ratio is 1:8, so that lentils are cooked after making provisions for water evaporation. (d) Stopping the gas supply after reaching the temperature of 98 °C (i.e., early shut off condition) and then retaining the enthalpy of the system can further reduce gas consumption and the required water quantity. Moreover, if the arrangement is such that the food item does not come in direct contact with the vessel wall that receives heat directly from the flame, burning of the food item can be avoided.

In view of these observations, some experiments were performed for further optimization of these ratios, and it is recommended for the case of rice that the water ratio be 1:2.3 with a gas flow rate of 4.3 mL/sec. If a higher flow rate is used (for shortening the time at the expense of efficiency), the recommended ratio is 1:3 at a flow rate of 7.3 mL/sec and 1:5 at a flow rate of 21.4 mL/sec. The same numbers of lentils are recommended to be 1:3, 1:4, and 1:8 for gas flow rates of 4.3, 7.3, and 21.4 mL/sec, respectively.

One important observation can now be emphasized. The water ratio increases with an increase in heat flux. For instance, the value of ratios of water to rice are found to be 2.3, 3, and 5 for heat flux numbers of 15,200, 25,830, and 75,720 kcal/h m^2, respectively. Similarly for lentils, the ratio was found to be 3, 4, and 8 for above-mentioned fluxes.

We would like bring to attention one more important point. The quantity of water required depends upon the quality of rice (possibly related to the amylose content of rice). When an inferior quality of rice is used, the ratio of water nominally increases to 2.35 $\pm$ 0.05. This value has been used whenever an inferior quality of rice has been used.

3.2.5. Water Ratio on Larger Scale. After studying the effect of water ratio for cooking on smaller scale, actual cooking experiments were conducted with rice, lentils, and potatoes with 72 L cooker model, and the results are shown in experiments 1, 2, and 3 in Table 5. As described in Table 5 of Part I, the pot size is D = 255 and H = 140 mm. The variety of food items used was "Wada Kolam" rice and "Arhar (tuvar)" lentils. Potatoes available from a local market were used. In experiment 1, the rice to water quantity ratio of 1:2, lentil to water ratio of 1:3, and potato to water ratio of 1:2 were used, as these were the optimized ratios at a laboratory scale for these available varieties. Each pot was charged with 6 kg of material. Lentils were kept in the bottom vessels (V_1), rice was kept in vessels V_2 and V_4, whereas potatoes were kept in vessel V_3. Twelve liters of water was added in the base. Heating was continued at the LPG flow rate of 90.4 mL/s for about 85 min. LPG consumed was 1060 g. Retention was allowed for 30 min.

Temperatures were noted during the heating and retention periods. It was observed that lentils and potatoes in all the vessels were nicely cooked to the required texture. However, smaller pockets of rice ranging between 100 and 200 g were observed undercooked in the central section of each of the pots. Rice in other parts was cooked. Also, temperatures of these pots were about 94 °C. This indicates that radial heat transfer was not effective up to the center of those pots. This was possibly because the water quantity was inadequate to cook this variety of rice. No excess water was left available for heat transfer. This resulted in an increased resistance to heat transfer to the center of the pot. Hence, experiment 2 was performed using a rice to water ratio of 1:2.5, whereas other ratios were kept the same. Heating carried out with a gas flow rate of 90.1 mL/s for 84 min consumed 1042 g

Table 5. Cooking Results of 72.0 L Cooker in PG Students Mess, ICT Mumbai[a]

	vessel				food + water (kg)							
E.N.	V_1	V_2	V_3	V_4	D	R	E.L. (kg)	heat time (min)	cool time (min)	LPG FR (mL/s)	G.C. (g)	remark
1	D	R	P	R	1.5 + 4.5	2.0 + 4.0	7.4	85	30	90.4	1060	uncooked rice pockets
2	D	R	P	R	1.5 + 4.5	1.7 + 4.3	7.2	84	30	90.1	1042	cooked sticky rice
3	D	R	P	R	1.5 + 4.5	1.8 + 4.2	6.9	83	30	89.8	1030	optimum water
4	D	R	R	D	1.4 + 4.6	1.8 + 4.2	7.0	85	30	90.8	1068	∼5 min more heating
5	D	R	R	D	1.4 + 4.6	1.8 + 4.2	6.7	85	40	87.3	1024	∼5 min more heating
6	D	R	R	D	1.4 + 4.6	1.8 + 4.2	5.2	85	30	86.1	1010	slightly more heating
7	D	R	R	R	1.4 + 4.6	1.8 + 4.2	5.8	85	30	88.1	1000	∼5 min more heating
8	D	R	R	R	1.4 + 4.6	1.8 + 4.2	5.1	82	35	86.6	980	adequate heating
9	D	R	R	D	1.5 + 4.5	1.8 + 4.2	2.2	85	30	82.7	970	sufficient heating
10	D	R	R	D	1.5 + 4.5	1.8 + 4.2	1.9	85	30	81.8	960	sufficient heating
11	D	R	R	D	1.5 + 4.5	1.8 + 4.2	2.1	85	30	81.1	950	sufficient heating
12	R	R	R	R	–	1.8 + 4.2	2.3	84	30	81.0	940	sufficient heating
13	D	D	D	D	1.5 + 4.5	–	1.9	86	30	82.2	970	sufficient heating
14	D	R	P	R	1.5 + 4.5	1.8 + 4.2	2.2	82	35	83.5	945	sufficient heating

[a] V: vessel (from bottom to top). D: dal (lentils). R: rice. P: potatoes. E.L.: evaporative losses. G.C.: gas consumption. E.N.: experiment number. Variety of food item: rice, Wada Kolam; dal (lentils), Tur (Arhar); potatoes, unchopped whole potatoes.

of LPG. It was observed that the lentils, rice, and potatoes were nicely cooked. However, the cooked rice was sticky and not completely free-flowing as required. This indicated that the water quantity in the rice was in excess. Hence, experiment 3 was performed using a rice to water ratio of 1:2.3 keeping the other ratios the same. At a gas flow rate of 89.8 mL/s for 83 min, 1030 g LPG was consumed. All the food items were nicely cooked. The rice was not sticky and was completely free-flowing. Hence, these ratios were maintained for future cooking experiments when the same quality grains were used. Some observations pertaining to the ratio of water to rice (for small scale) have been given at the end of Section 3.2.4. Similar observations also hold for large scale cooking.

The foregoing discussion brings out the optimum water quantity for 180 and 255 mm diameter pots. Some experiments were performed on even larger scales, and pots of 280 and 330 mm diameter were employed. Following are the observations: (a) The 280 and 330 mm pots can cook 2 and 4 kg rice, respectively. If the rice quantity is less than 25%, then it remains uncooked. (b) For all sizes (180, 255, 280, and 330 mm), when the initial rice quantity is more than 50% of maximum capacity of the respective pots, the rice to water ratio was found to be 2.35 ± 0.05.

In the foregoing discussion, the problem of the uncooked portion was solved by using additional water. As discussed in Section 2.4, some portion of rice remains uncooked because of temperature stratification. In view of this, some hardware changes have been proposed in place of using an additional quantity of water.

3.2.6. LPG Consumption for Cooking. In order to optimize the gas consumption to cook a full charge of the cooker, experiments were performed for different combinations such as (i) only rice, (ii) rice and lentils, (iii) only lentils, and (iv) rice, lentils, and potato. The total thermal load was 72 kg of cooking material and water and 15 L water in the base. Heating was carried at a 85 ± 5 mL/s gas flow rate and respective gas consumptions were calculated. Temperatures of charges in the different pots were also noted. To reduce gas consumption further, lentils and rice were allowed to presoak for some time. All these results are shown in Table 5 as experiment numbers 4−14. It is observed from this table that the optimum is to use 940 g of LPG to cook 22 kg of rice, 950 g of LPG to cook 9 kg of lentils and 11 kg of rice, 945 g of LPG to cook 4.5 kg of lentils, 11 kg of rice, and 6 kg of potatoes, and 970 g of LPG to cook 18 kg of lentils. In general, gas consumption to cook a full charge is about 955 ± 15 g.

At these conditions, lentils could be easily mashed after cooking. Rice was very nicely cooked and was completely free-flowing. Potatoes were also nicely cooked and could be peeled very easily. All the cooked food items had better taste, flavor, and appearance compared to those cooked in the conventional way. This finding was based on a survey of the opinion of 300 student members of the mess. Heating time is about 85 min and retention time is 30 min. If the gas flow rate is further reduced, heating time would increase, and that may act as a constraint in the overall timetable of the hostel mess.

The effect on thermal efficiency of a cooker with a (i) flow rate of LPG and (ii) distance between the burner and cooker base are discussed in more detail in Part I (Sections 4.5 and 5.5, respectively).

3.2.7. Extent of Cooker Usage. Taking into consideration that the cooker may not be used with a full charge every time, experiments were conducted for different charges, e.g., 3, 4, and 5 L in each pot (i.e., 50%, 66%, and 83% of full capacity of the cooker) and again temperature profiles were studied. It was observed that heating and retention cooling profiles were similar to those observed for a 72 L charge as shown in panels (A) and (B) Figure 14. At the LPG flow rate of 85 mL/s, the time to reach the boiling temperature, the gas consumed, and the efficiencies for different capacities are shown in Table 6. It is observed that although the efficiency increases with an increase in charge, there is no significant difference between the efficiency values for different charges.

3.2.8. Effect of Geometry. Experiments were also carried out using various geometries of cooking pots/vessels such as cylindrical, triangular, square, and rectangular. The dimensions are shown in Table 7. Initially experiments were carried out using cylindrical

pots, which are readily available in the market. A cooker of 120 L capacity accommodates 15 pots. Fourteen pots were charged with 8 L water, and one pot was charged with 2 kg rice with a 1:2.5 as rice to water ratio. LPG flow rate was maintained at 1.1 kg/h. Heating was continued for 15 min after a steam puff comes out from the base (approximately 60−70 min). The retention period was maintained constant (40 min).

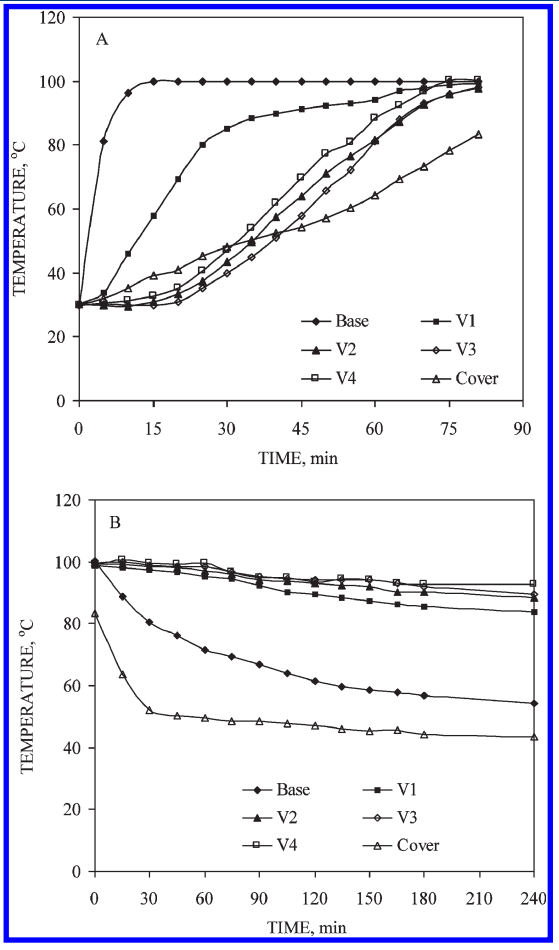

Figure 14. Temperature profiles for water in base, vessels, and cover for sunbeam type burner: (A) heating, (B) cooling.

3.2.8.1. Cylindrical Vessel. It was observed that good quality rice (quality of the rice has been measured in terms of its market price), about 50 cents per kg, is cooked nicely. However, low quality rice (Rs. 35 cents per kg) remains partially uncooked. Therefore, attempts were made to cook this poor quality rice by increasing the water to rice ratio. The increase in ratio, however, results in mushy rice. It was thought that an increase in the heat transfer area to volume of vessel (Table 7) may help to cook the rice, and hence, various geometries were tried. Further, variation of the rice to water ratio for a given quantity of rice was also studied for low quality rice. All experiments were carried out using low quality rice unless otherwise specified.

3.2.9. Other Aspects. In addition to the various parameters affecting the cooker performance discussed, additional factors were studied for making it user-friendly and more acceptable.

3.2.9.1. Pot Design for Cooking and Dispatch. In all developing countries including India, large numbers of charitable institutions along with various government bodies offer free food, mainly rice and lentils or khichdi (mixed food containing rice, lentils or other cereals, vegetables, and spices), to school/underprivileged children (about 110 million in India). The process involves managing and handling of large food quantities. Conventionally, large vessels are used to cook the rice by boiling (open pan, drain method) as described before. It is then packed in small containers (∼15 kg) and dispatched to the respective destinations. The overall process including removal of cooked rice from large cooking vessels and then distributing it again is a labor intensive and particularly unhygienic step. This problem could be addressed with better design of cooking pots that would allow cooking and dispatch of the food in the same container. Two methodologies were tested for this purpose.

Because the open pan method is widely followed at almost all places with large burner flow rates, heat losses are significant. This causes low thermal efficiency and high consumption of fuel that in most cases of community cooking is LPG. For example, at Ratnanidhi Charitable Trust, Girgaon, Mumbai, ∼200 kg of rice and 125 kg lentils are cooked per day. Both rice and lentils are cooked by the method described above, with three large burners and three cooking vessels. Multiple cooking batches are required daily for cooking of the said food quantities. The fuel consumption is 75 LPG cylinders (capacity 14.2 kg) per month. Thus, the cooking efficiency is in the range of 25%. The use of our cooker

Table 6. LPG Consumption and Efficiency for Different Charges in 72.0 L Cooker

S.N.	charge in vessels (L)	time of heating (min)	LPG consumption (g)	η_{therm} (%)
1	36	45	524	71.4
2	48	55	643	71.5
3	60	67	788	71.8
4	72	82	960	72.1

Table 7. Particulars of Various Geometries of Cooking Vessels[a]

	dimensions		volume	surface area	volume/surface area
geometry	D/L/B (mm)	height (mm)	$\times 10^{-3}$ (mm^3)	$\times 10^{-3}$ (mm^2)	$\times 10^{-1}$ (mm)
square	260/280	300	21870	3865	5.66
triangular	240	200	5985.95	1938.82	3.09
cylindrical	280	150	9231.6	1495.425	6.17
	350	200	19232.5	2512	7.66

[a] For square vessel, lower side = 260 mm, upper side = 280 mm. For triangular vessel, base = 240 mm, height = 200 mm.

would save at least 45 LPG cylinders per month. Three cookers of 120 L capacity each were supplied to this site, and a successful cooking demonstration was given for one cooker. Though the cooker worked nicely, it contained 15 of the 8 L pots. The 8 L capacity was considered to be small. Because of the specific requirement of cooking and transport in the same pot, pots with a square base were designed similar to those of the 700 L cooker (Figure 18 of Part I).

In addition to fuel saving, there is an advantage in food distribution and transport. There is no need to remove the cooked food from the cooking pots and reload it in other vessels. Also, because of the specific pot design, they can be properly arranged in the transport vehicle. A full charge cooking trial was performed on a 160 L capacity cooker with these pots. Twelve pots were arranged in four stacks of three pots each. Though the full capacity of the pot is 14.4 L, it is necessary to allow for swelling of the cooked food. Hence charging was done accordingly. All of the four bottom pots were charged with 3 kg of lentils and 9 kg of water, 7 pots were charged with 3.5 kg of rice and 9.625 kg of water, and the remaining pot was charged with 3 kg of rice and 8.1 kg of water. The rice used was of low quality with a relatively low price. Twelve kilograms of water was charged in the base. It was found that both rice and lentils got cooked nicely, though the cooked rice was sticky in nature. It can be said that this is mainly due to the quality of rice. It is always found that good quality rice is always free-flowing in nature and low quality a little bit sticky. This may be due to non-uniformity of initial moisture content in the low quality rice in addition to the mixing of two varieties of rice. Thermal efficiency of the system was found to be 73%. Replacement of present cooking practice by this cooker at Ratnanidhi Trust could result in LPG savings of 45 cylinders/month worth $300/month (with rate of LPG at $6.67 per cylinder). It may be mentioned that the cost of one cooker is about U.S. $630. With 20% depreciation and 10% interest, the payout period works out to be less than eight months.

Another option is cooking in small food containers like tiffin carriers. This can be useful at places where only rice and lentils (or a khichdi-like item) are to be supplied. In cooking of lentils, it is normal practice to cook (boil) the lentils first and then perform the tadka (frying process with vegetable oil followed by addition of spices separately spluttered in oil). This process requires extra effort as well as extra fuel. Instead of this, the ingredients for tadka (oil, spices, etc.) may be mixed well and added to the cooking material prior to cooking. This would avoid the reprocessing of lentils after cooking, and hence, the only required operation would be to distribute the separately prepared tadka (or plain raw spices and oil depending on choice) prior to cooking along with the soaked lentils in the containers. For applications involving khichdi-like preparations, it is necessary to distribute appropriately mixed grains and other ingredients to all containers of the tiffin carrier. Thus in both of these applications, there is no secondary processing operation such as tadka, remixing, etc. Once the cooker is opened, the food is ready for direct serving. Two sizes of tiffin carriers (6 and 12 L capacities) in the 24 L cooker were used for testing. The 24 L cooker was used because it was found adequate to hold three small tiffin carriers. It should be noted that a lot of space remained unutilized inside the cooker. A domestic LPG stove was used as a heating source with a large burner at maximum flow rate (~3 g/min or 21.74 mL/s) for all experiments. Three carriers of small capacity were used at a time, while in the case of the larger one, a single tiffin carrier was used. Both small and large carriers have four containers each having a volume of about 0.6 and 1.7 L for small and large carriers, respectively.

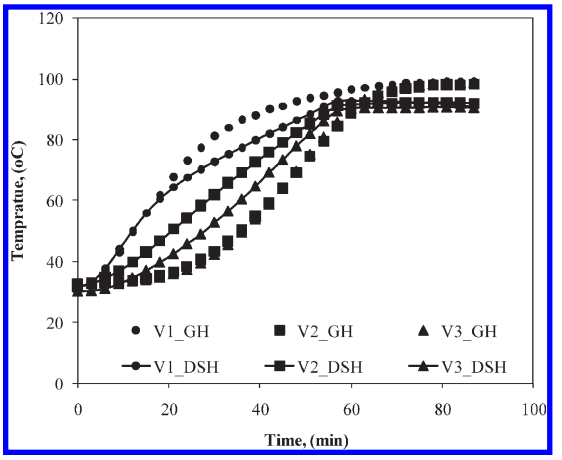

Figure 15. Comparison of temperature profile for vessels for two modes of heating. DSH: Direct steam heating. GH: Gas heating.

Thermocouples were placed at the center of each container, in the base, and on the outer cover to measure temperatures. Water quantities were monitored before and after the experiment for evaporative losses. Typical temperature profiles were found to be similar to that for the cooker itself. On average, thermal efficiencies obtained for small and large tiffin carriers were 66% and 59%, respectively. These values are quite low compared to the possible efficiency of the standard cooker. This may be due to the fact that the complete capacity of the cooker was not utilized. The height of small and large tiffin carriers is 140 mm and 217 mm, respectively. When this is compared to the height of the cooker (575 mm), it is observed that the extra height provides additional surfaces for heat loss. Three carriers occupy almost the entire base area, while a single large carrier uses less than half the base area. This combination when compared to the 24 L cooker suggests that heat losses remain the same in both cases and hence result in the lowering of net thermal efficiency at lower inner container capacities. This limitation can be overcome with proper sizing of cooker and tiffin carriers for such a cook-and-dispatch operation.

3.2.9.2. Direct Steam Injection. Though the cooker is presently standardized with LPG as fuel, it can also be used with other fuels like biomass or with an external steam supply. The option of external or direct steam supply was investigated keeping in mind that steam could be available from any other efficient steam generation method where the overall system efficiency would be higher. Also, another option for steam generation comes from the use of a renewable source such as solar energy. The option of using solar generated steam would mean a completely CO_2 free and highly efficient cooking practice.

An external steam supply option was investigated using a 160 L cooker with 15 vessels. Fifteen vessels were arranged in five stacks, each stach having three vessels, V_1, V_2, and V_3. Steam was introduced inside the cooker through 2.5 cm diameter holes, drilled at the center of the inner and outer cover. Stacks of vessels were arranged such that steam was hitting the base and not any the vessels directly. Steam was generated at a rate of 25 kg/h using an oil-fired boiler. Figure 15 depicts the comparison of temperature for vessels V_1, V_2, and V_3 for two different mode of heating: gas heating and introduction of direct steam-generated heat using a boiler.

Temperature profiles for the vessels clearly suggest that 10−15 min of cooking time can be saved by direct introduction of steam. Vessel V_1 is heated at a same rate for both modes of heating in the initial few minutes.

Testing of the direct steam supply to the cooker was done using the 24 L cooker and a tiffin carrier of 12 L. Steam used was saturated steam at 100 °C and was generated using a 6 L pressure cooker after removing the cooking vessels and the whistle weight. Steam coming out from the nozzle at the top of the pressure cooker was fed to the cooker once a steady steam rate was obtained. Because the heat is to be supplied by steam, a hole was drilled through the two covers of the cooker for steam injection through a pipe that released steam near the bottom of the cooker. The diameter of the hole was selected so as to match the size of the steam injection pipe. The steam rate obtained was 45 g/min.

It was observed that although the temperature of vessel V_1 rises faster than the other vessels, it is no longer as fast as that for the regular cooker with heating by a flame below. The reason for a smaller difference between the temperatures of V_1 and the other vessels is that steam is available for heating to all the vessels simultaneously. Whatever small difference is there is possibly due to following reasons. Vessel V_1 has the largest area available for steam condensation (extra bottom surface), and steam was injected near the bottom pot. The temperature rise for vessel V_3 is the slowest followed by vessel V_4. The temperature of the base is actually the temperature of condensate accumulated. Because the base is directly exposed to the surroundings, it also loses heat. The time required to reach the desired temperature levels was 40 min. Actual heat input to the cooker was calculated from the steam flow rate and time of experiment as

$$\text{Heat Input} = \text{rate of steam supply} \times \text{latent heat} \times \text{time}$$

The thermal efficiency of the cooker was calculated considering the heat given out by steam and that gained by the cooker and was found to be 84.5%. The efficiency for pots (i.e., water kept in the containers of the carrier) was 74.2%. For very large scale cooking systems providing a few million meals per day, steam is generated using industrial boilers, and it is then used for cooking. This experiment shows that if steam is available by external means, it can be used more efficiently in the cooker, and there is further scope for improvement in thermal efficiency in large scale cooking.

3.3. Comparison of Present Cooker with Other Cooking Devices. Some of the cooking devices available in the market are the pressure cooker, Chakson cooker, Sarai cooker, and Mallick cooker. These models are capable of cooking common food items such as rice, lentils, and vegetables. The performance of the present cooker has been compared with pressure and Chakson cookers in terms of energy saving, capacity, scalability, ease of operation, and food quality. Other cookers use coal as a heating source and are not discussed here.

3.3.1. Pressure Cooker. A pressure cooker is a device that cooks food items using steam pressurized at 0.2 MPa and 120 °C. It is mostly operated on commercial fuels such as LPG, kerosene, and coal. It is available in the market in capacities ranging from 2 to 30 L of the outer vessel. The actual capacity of the cooking vessel is generally 70−75% the capacity of the outer vessel. Comparison of the optimum water quantity to be added to the food items and the energy saving aspects are discussed in Sections 3.2.5 and 3.2.6. The present cooker can be scaled up to large capacities, unlike the pressure cooker, and the 72 L capacity is being successfully operated at about 50 locations in India.

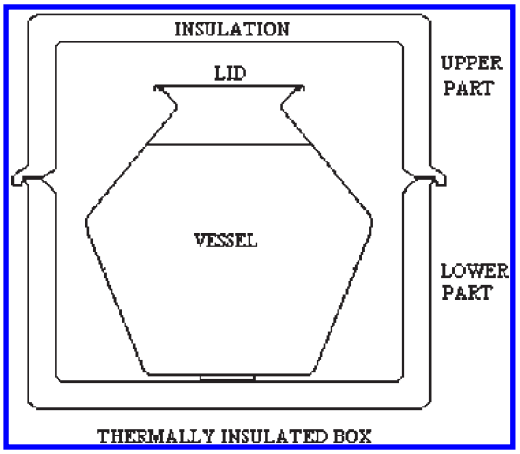

Figure 16. Schematic of chakson cooker.

3.3.2. Chakson Cooker. A Chakson cooker is the patented product of Anna Aluminum Private Limited, Kerala. It utilizes a 5 L capacity vessel with lid and thermally insulated box. The schematic of the cooker is shown in Figure 16. The insulated box is double walled and consists of 12 mm thick thermocole (polystyrene foam) as insulation between the walls. Food material, along with an excess quantity of water, is put in the pot, which is then heated to boiling point. The mixture is stirred two or three times during heating as per requirement. When the boiling point is reached, the pot with lid is put into the lower part of the insulation box. Both parts of the box are tightly fitted creating a closed system. Retention is allowed for a much longer period, and the box is opened when food is served.

3.3.2.1. Chakson Cooker versus Present Cooker. As both cooking devices work on similar principles of boiling the contents and retention, it was thought desirable to compare the retention/cooling processes. Figure 17 shows the cooling period comparison between vessels V_2 and V_3 of the 4.5 L capacity cooker and the 5 L capacity Chakson vessel during the retention period. It is observed that vessels of the present cooker cool slower than the Chakson pot, thus showing better performance. In the Chakson cooker, only one item can be cooked at a time compared to four items in the present cooker. Taste and nutrition is preserved in both the models. Food can be kept warm for at least 20 h. Heating efficiency of the Chakson pot varies from 50.5% at a 21.4 mL/s flow rate to 56.7% at 5.6 mL/s flow rate, which is lower than that for the present cooker which in the range of 65−75%. The Chakson cooker can cook a maximum of 1 kg of rice at a time. This would require 90 g LPG to cook 1.5 kg of rice compared to 60 g for the present cooker at similar LPG flow rates.

3.3.2.2. Effect of Insulation Material. The present cooker utilizes a 5 mm width air gap between the two covers for 24 L and 12 mm for 72, 120, and 160 L cookers as insulation to reduce convective heat losses. It was thought desirable to investigate the effectiveness of the same insulation principle in a Chakson cooker. Hence, a Chakson cooker was modified to accommodate a thermal insulation box having a 5 mm wide air gap between the two walls. A 5 L water charge was used in the vessel. The vessel was covered with a lid. Water was heated from room temperature of 27 °C to 99 °C at a LPG flow rate of 21.4 mL/s.

As soon as the water charge reached a temperature of 99 °C, heating was discontinued. The vessel was put in the cooker box,

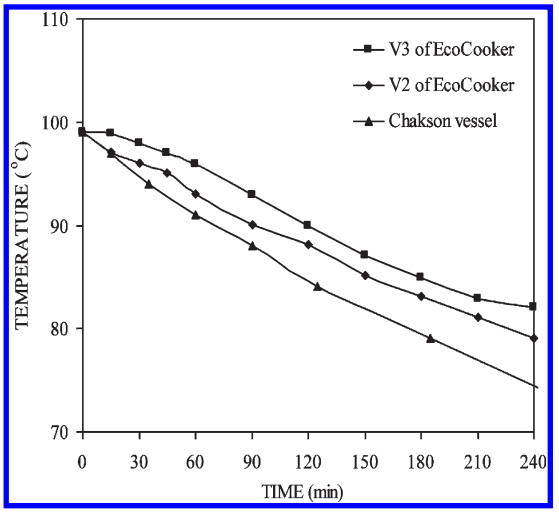

Figure 17. Comparison of temperature profile during cooling. V_2 and V_3 are the vessels in the cooker.

and the box was closed. Temperatures of water, air inside the box, and the outer wall of the box were measured using thermocouples during a period of 6 h.

In both cases, temperatures of the water charge after 6 h of retention showed a similar cooling trend with the temperature in the former case higher by 2 °C over that in the latter case. Air temperature where thermocole was used as insulation is higher compared to the air temperature using an air gap as insulation. The outer wall temperatures of the air-insulated box were higher by about 10 °C compared to those of the thermocole-insulated box.

There was little difference between the water temperatures for the two cases, indicating an equal rate of heat loss to the surroundings. The maximum temperature of air and outer wall for the air-insulated box are 64 and 46 °C, respectively, whereas for the thermocole-insulated box these were 71 and 37 °C, respectively. The outer wall temperatures in both cases are in line with the established industrial norms for an insulated outer surface.

According to optimization described in Section 2.2, the air gap thickness that prohibits the formation of natural convective currents in this temperature range is estimated to be in the range of 5 mm. The difference between the respective inner and outer wall temperatures of the two boxes pertains to the differences in thermal conductivity and thickness of insulation. The thermal conductivity of air is 0.028 W/m K (average) and of thermocole (polystyrene foam) is 0.04 W/m K, and their respective thicknesses are 5 and 12 mm. Assuming similar heat transfer coefficients, thermocole thickness equivalent to 5 mm air thickness is about 7 mm. Compared to the air gap, the additional 5 mm thickness of thermocole improves performance in reducing heat transfer from the inner wall to outer wall. This results in the difference between the respective inner and outer wall temperatures of the two different insulating materials.

4. RENEWABLE SOURCES OF ENERGY

4.1. Solid Fuel. *4.1.1. Preamble.* In the past, traditional sources of energy such as fuel wood, charcoal, dung, etc. were the only sources of energy used for all types of applications. It is only during the last 250 years that fossil fuels such as coal, oil, and gas have emerged as major sources of energy in most developed countries, and it is during this time that electricity has also begun to be used for cooking. However, nearly 75% of the world's population lives in developing countries, and the majority of it continues to depend on traditional sources of energy for most of its energy requirements. In the last few decades, these developing countries have experienced a rapid depletion of natural forest resources that has resulted in hardship for the people living in rural areas, especially women and children who spend a considerable part of their time and energy in search of fuel wood and biofuels, and they often have to cover long distances. In particular, the domestic sector relies heavily on traditional sources of energy, mainly for cooking, for which traditional stoves are often used. These stoves are usually thermally as well as environmentally inefficient and hence create drudgery as well as problems for the users.

4.1.2. History. In earlier ages, cooking was presumably done over an *open fire* with fuel arranged in a pyramid configuration. This mode of cooking, primarily for roasting meat, had major drawbacks: dispersion of the flames and heat during windy conditions, lack of proper control over the fire, exposure to heat and smoke, as well as fire hazards. However, at the same time, heat and smoke had also certain benefits such as food preservation and/or protection against large animals, insects/rodents, and providing warmth during the cold seasons. A major step toward the evolution of other cookstoves (Chulhas) was the development of pots of various shapes and sizes. This necessitated the modification of the open fire to create *shielded fires* in order to balance the pot over the fire. The simplest form of the shielded fire was a three stone arrangement in which stones were arranged at approximately 120 degrees to one another on level ground. Besides allowing a cooking pot to rest firmly on it, this arrangement also partly saved the fire from the vagaries of wind and slightly increased cooking efficiency. However, by and large, the three stone fire still suffered similar drawbacks as the open fire. Subsequently, the shielded fire was changed to a U-shaped mud or mud/stone enclosure with an opening in the front for fuel feeding and combustion air entry. Three small humps (made of the same mud material) were put on the top rim of the enclosure and acted as a pot rest, provided an induction point for secondary air needed for better combustion of volatile matter, and provided an exhaust gas exit. In order to conserve heat from the hot flue gases and to enhance cooking productivity, additional pot holes were later added. These pot hole enclosures were connected by a tunnel. All the above-mentioned innovations in cookstove design were made mainly by users in the light of their own experience. These innovations did increase the efficiency of the stoves to some extent, but health and other safety hazards remained.

4.1.3. Improved Chulhas. In pursuit of the conservation of fuels, governments of the developing world launched national programs on improved chulhas (cookstoves). The following are the criteria for efficient cooking operation: (1) simple construction and easy fabrication, (2) easy operation and maintenance, (3) easy ignition (4) complete fuel consumption, (5) higher retention time of flame inside the hearth, (6) higher heat transfer to the pot, (7) less pollution and soot formation.

Under these programs, many designs were developed by various agencies. Here, we discuss two that satisfy most of the above-mentioned criteria and can be considered as representative of recent developments: Harsha stove and Oorja stove.

We have selected these two cookstoves for further experimentation for use with the cooker developed in Section 6 of Part I. A Harsha stove operates in continuous mode, which means fuel can be charged continuously until the cooking process is complete,

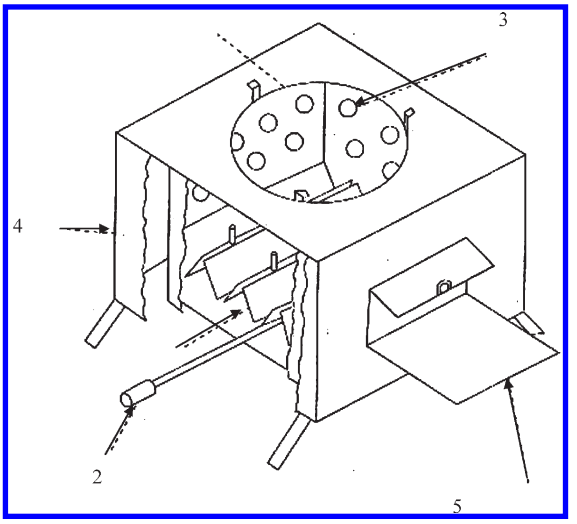

Figure 18. Schematic of Harsha stove: (1) corrugated grate, (2) ash scraper, (3) perforated combustion chamber, (4) air jacket, (5) fuel feeding hole.

whereas the Oorja stove operates in batch mode, where a sufficient quantity of fuel is loaded initially, so that a particular cooking operation is completed. This was another reason for selecting the Harsha and Oorja stoves, so that cooker can be tested with both continuous and batch mode stoves.

4.1.3.1. Harsha Stove. The model was developed in 1990 at the Technical Back-up Unit, Regional Research Laboratory (CSIR), Bhubaneswar, Orissa. This stove is capable of burning a variety of fuels containing 1−40% ash and high volatile materials such as firewood, leaves, twigs, dung-cakes, agricultural waste, raw coal, charcoal, etc. The stove is schematically shown in Figure 18. It consists of a corrugated grate, ash scraper, perforated combustion chamber, air jacket, and fuel feeding hole for flow of air in primary and secondary streams. The combustion air is preheated through the hot surfaces of the stove before it is drawn into the stove by natural draft during burning of the fuels, which occurs in two stages. Fixed carbon and volatile components of the fuel burn in the corrugated grate and in the perforated combustion chamber of the stove, respectively, with the help of preheated primary and secondary air streams to obtain complete combustion with low excess air. Fuel can be charged continuously through the fuel-feeding hole. The ash scraper helps to remove ash intermittently during burning of high ash fuels. Otherwise, ash discharges automatically from the stove. A high temperature clean flame (800 °C) with reduced smoke is obtained during the combustion of solid fuel.

4.1.3.2. Oorja Stove. Panel (A) of Figure 19 shows the schematic of the Oorja stove. It consists of a combustion chamber of an inner diameter of 108 mm and a height of 175 mm. A sufficient amount of solid fuel (biomass pellets) is placed inside the combustion chamber initially for a particular cooking process. The ash collector is inserted in the combustion chamber for the collection of ash. This stove works on the principle of forced draft, which is created by using a battery operated fan at the bottom of the combustion chamber. The fan can be operated at different speeds by using a voltage regulator. Although the forced draft is upward, the flame front travels from the top down.

Air passes through the combustion chamber in two ways: first, as primary air through the bottom of the fuel bed, and second,

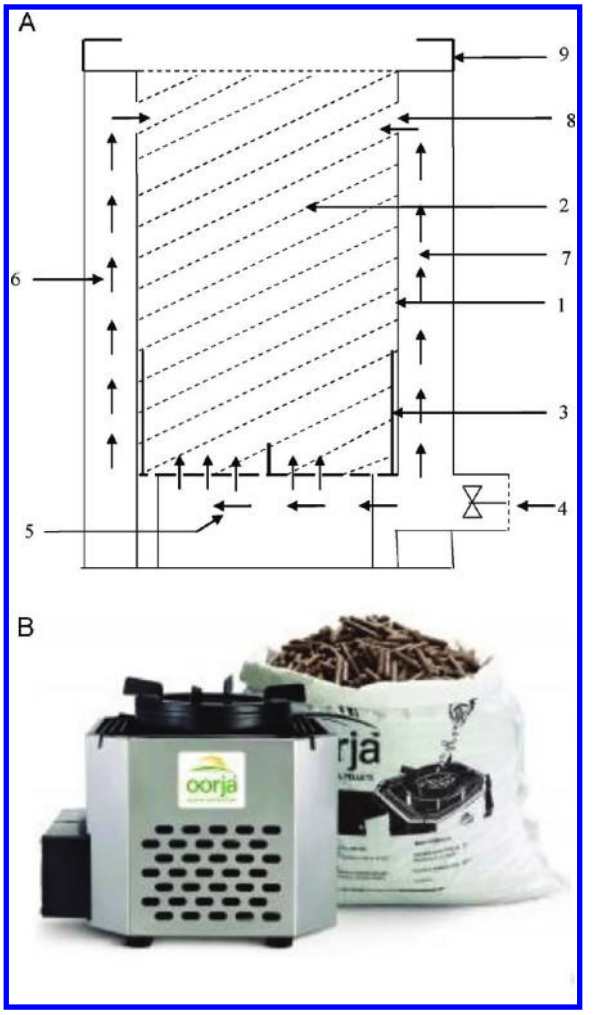

Figure 19. Oorja stove: (A) schematic, (1) combustion chamber, (2) solid fuel, (3) ash collector, (4) battery operated fan, (5) primary air, (6) secondary air, (7) annulus for flow of secondary air, (8) holes, (9) stand. (B) photograph.

as preheated secondary air at the top of the bed, which comes through the annulus formed between the combustion chamber and the external wall of the stove. There are 18 holes of 5 mm diameter for the emergence of secondary air into the fuel chamber at the top. To keep a pot on the stove, a stand is provided at the top of the stove. The Oorja stove is shown in panel (B) of Figure 19.

4.1.4. Experimental Setup and Procedure. The experimental setup is essentially similar to that in Figure 1 of Part I except the gas burner was replaced by a stove burning solid fuel. To simulate cooking performance, experiments were performed with water as the charge. Casuarina wood was tested as fuel for the Harsha stove, and biomass pellets were used as fuel for the Oorja stove. Wood was cut into 50 mm × 50 mm × 500 mm pieces. Biomass pellets used had a cylindrical shape, with 11 mm diameter and length varying up to 60 mm.

The 24 L cooker was used with the Harsha stove, and the 5 L cooker was tested with the Oorja stove. The standard Harsha stove is too big for the 5 L cooker, and the standard Oorja stove is too small for the 24 L cooker, which is why different sizes of cookers were used for the two different stoves. Four pots of 7 L were used with the 24 L cooker, and three pots of 1.5 L each were used with the 5 L cooker.

Small wood pieces were kept over cotton waste soaked in kerosene in the combustion chamber of these stoves for ignition. After ignition in the Harsha stove, normal sized feed was placed over the fire for burning. In the Oorja stove, the fuel was already in place under the cotton waste. Once the emanating smoke stopped (after about 30−40 s in the case of both wood and biomass pellets) and there was a steady flame, the cooker was placed on the stove. Thermocouple probes were inserted in the water in the base and in the pots to measure temperatures of the charge inside.

The flame diameter in case of both wood and biomass pellets was about two-thirds of the base diameter of the cooker. Fuel was charged from time to time according to requirement for the Harsha stove, such that continuity in the flame was maintained. Initial water temperatures in all cases were 30 ± 1 °C. The cooker contents were heated until they reached near boiling point. In this case, temperatures of 98 ± 1 °C for vessel V_1, 97 ± 1 °C for vessel V_4, and 95 ± 1 °C for vessels V_2 and V_3 were allowed to be achieved, just like the end-of-heating condition when testing the cooker with LPG as a fuel. At this point, unburnt fuel was taken out and immediately extinguished with a little quantity of water. The cooker was immediately opened to avoid condensation of the steam formed. Initial and final quantities of fuel as well as water in all the pots and the base were measured to a precision of 0.005 kg on an electronic balance to estimate the fuel consumption and water loss due to evaporation during heating. Temperatures of the various components during heating were measured at fixed time intervals to evaluate the heating performance of the water charge with a precision of 0.1 °C. The overall thermal efficiency was estimated using eq 1.

4.1.5. Results and Discussion. Calorific value for Casuarina wood is 4425 kCal/kg and that for biomass pellets is 3900 kCal/kg.

4.1.5.1. Harsha Stove. The first experiment was carried out using 50 mm × 50 mm × 500 mm sized fire wood pieces for which the burn rate was found to 1.9 kg/h, which corresponds to 63,000 kCal/h m^2. With this flux, the efficiency of the cooker obtained is 31%. The optimized flux for the cooker is 21,000 kCal/h,m^2 when it is operated with LPG as the fuel. The obtained flux (63,000 kCal/h.m^2) is much higher, so another experiment was carried out with a reduced burn rate of 1.1 kg/h (38,000 kCal/h m^2), for which the efficiency of the cooker was also 31%.

4.1.5.2. Oorja Stove. The 5 L cooker was tested with the Oorja stove, using biomass pellets as a fuel. The burn rate for the experiment was 0.48 kg/h, which corresponds to a flux of 63,000 kCal/h m^2. With this flux, the efficiency of the cooker was found to be 40%.

4.2. Solar Energy. During the past 80 years, several designs of cookers have been proposed. The focus of development has been to improve the energy efficiency and also to increase the cost effectiveness of the solar cooking systems. Solar cooking has been found to produce more nutritious food than is obtained by conventional methods and in the pressure cooker.[32−34] There are two types of solar cooking devices: oven type solar cookers (solar box cooker) and concentrating type solar cookers.

4.2.1. Oven Type Solar Cookers. This type of cooker is essentially an insulated box with sides blackened from the inside and a transparent glass cover on top. These are the closed units working on the principle of the greenhouse effect. Glass is transparent to energy in the solar spectrum, which is mostly in the visible and short wavelength infrared regions, and glass is opaque to blackbody radiation, which is long wavelength infrared. Sunlight enters the oven through the glazing and heats the inside black-colored high absorptivity and low emissivity surfaces. Cooking pots are also painted on the outside with high absorptivity and low emissivity materials so as to absorb the solar energy. Glass's opacity to the blackbody radiation emitted by the contents and interior of the oven results in increasing of temperature inside the oven. This heat is utilized for cooking of the food items. The advantage of these cookers is simplicity of operation and economy, as they are affordable to common people. However, these cookers cannot be used to generate higher temperatures. The efficiency of the system is also low, as the system cannot track the movement of the sun. In order to enhance the performance of the cooker, one or more of reflectors (boosters) need to be added. Danao and Joshi[33] have described the pertinent aspects of box type cookers.

4.2.2. Concentrating Type Solar Cookers. This type of solar cooker consists of a concentrating reflector that focuses the incident solar rays at a particular point or locus of points. The receiver or heating target is kept at the focus and receives the rays. Usually, the receiver is coated with high absorptivity material. The heat received is transferred to the material inside the receiver that is heated. Higher temperatures can be achieved in these cookers, and the cooking time can be reduced. The temperatures are proportional to the ratio of the aperture of the concentrating reflector to the focusing area. However, these type of cookers need tracking to follow the sun during the operating time interval so as to intercept the maximum amount of solar energy. Hence, their operation becomes relatively difficult and needs skill. Paraboloidal concentrators with a vertical cylindrical receiver have been successfully used are very popular for the direct application of cooking. Danao and Joshi[34] have discussed the design and optimization features of this type of solar cookers.

Wolfgang Scheffler is the inventor and promoter of Scheffler Community Kitchens (large parabolic dishes for community kitchens, bakeries, etc.[35]). Over 2000 large cookers have been built, commissioned, and distributed worldwide by 2008. The small scale Scheffler dish-based cooking system consists of a dish (which is a segment of a paraboloid), a secondary reflector, and the cooking vessel. Incident rays from the sun are reflected from the Scheffler dish onto the secondary reflector that directs these rays onto the bottom of the cooking pot. Community-scale cooking systems consist of a number of Scheffler dishes with their focus on the receiver where steam is generated. The steam is carried through a common header to the kitchen for use in the cooking process. During the past 80 years, several designs of cookers heve been proposed. The focus of development has been to improve the energy efficiency and also to increase the cost effectiveness of the solar cooking systems.

In Section 3, LPG gas was employed as a fuel. In this case, a detailed optimization exercise has indicated that the flame size should be one-third of the diameter of the cooker base. It was also found that the optimum flux is about 25,000 kCal/h m^2. It was thought desirable to investigate the possibility of solar energy. An attempt has been made to achieve the optimum value of heat flux using solar energy. It may be noted that solar energy can be focused on a concentrated hot spot geometrically similar to the projection of the flame produce by stove (burning either LPG or solid fuel).

The schematic arrangement of solar energy is shown in Figure 20. It consists of a primary reflector, secondary reflector, and cooker of 24 L size. During operation, there was a need for tracking that was carried out every 10 min. For the 24 L cooker

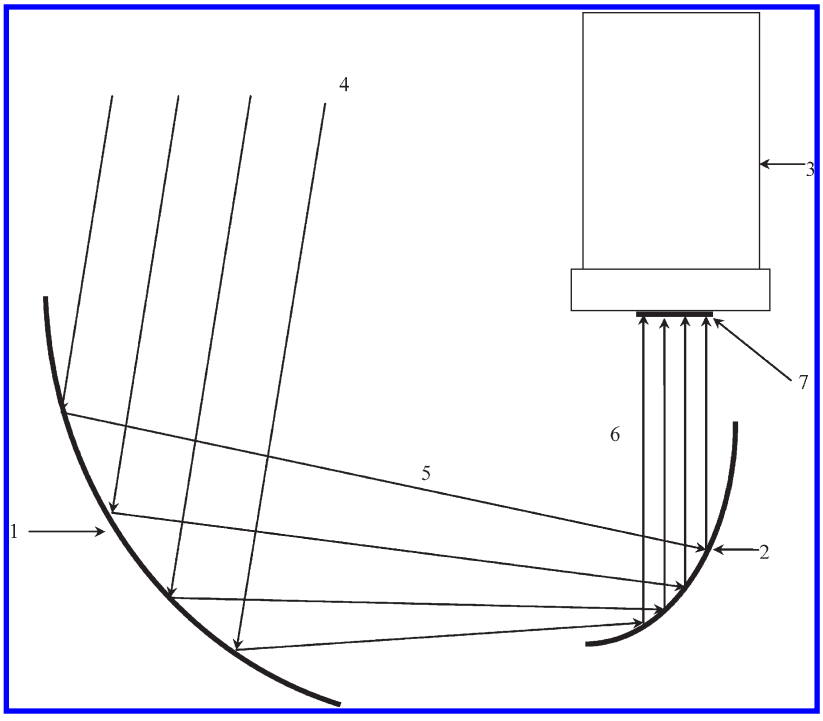

Figure 20. Schematic arrangement of a cooker using solar energy: (1) primary reflector, (2) secondary reflector, (3) cooker, (4) rays coming from sun, (5) rays reflected from primary reflector, (6) rays reflected from secondary reflector, (7) hot spot at cooker bottom.

(base diameter = 400 mm), the optimum heat transfer rate is calculated to be about 2,500 kCal/h or 2.9 kW. The average efficiency of the reflectors was found to be 90%, and the efficiency for absorbers was found to be 50−60%. Thus, the overall efficiency is calculated to be in the range of 45−55%. Thus, for a power requirement of 2.9 kW and a DNI value of 600 W/m^2 ,the area of the primary reflector would be about 10 m^2. Further work is in progress in regard to increasing the energy efficiency.

5. CONTINUOUS COOKING

5.1. Preamble. Section 3 shows that the energy required for cooking is mainly needed to increase the temperature from ambient to about 98 °C. The actual energy required for the cooking reaction is a small fraction of the sensible enthalpy. Because cooked food is available at 98 °C and is consumed at temperatures below 50 °C, a major portion of the sensible enthalpy can be recovered. A brief summary of the previous work on continuous cooking will now be described.

Various methods for cooking of grains (especially rice) on a continuous basis have been patented. Sugimura[36] developed a process for continuous cooking of rice by steam. This process involves first heating of rice in a steamer thereby promoting its gelatinization, followed by heating in hot water, and again steam cooking for a short time in a continuous manner. The process claims to obtain full grain well-cooked free-flowing rice.

An automatic and continuous rice cooking system developed by Watanabe[37] consists of a spiral rotary steam vessel with an elongated steam jacket having a semicircular bottom, screw conveyer, and steam tunnel passage provided with a mesh conveyer. The overall process involves three steps: (a) steaming process in which starch is released from the rice, (b) a gelatinization process in which the starch from the rice is gelatinized, and (c) an adsorption process in which the gelatinized starch is adsorbed by the rice grains.

The process developed by Miyagawa et al.[38] claims to be adaptable for various kinds of raw rice and a variety of textures for the finally cooked rice. It essentially uses a conveyor belt arrangement for moving the rice. The authors have used water-soaked rice for experimentation. The system has three sections. In the first section, the presoaked rice was preheated to cooking temperature. In section 2, rice was allowed to cook, and steam supply was not needed. However, in section 3, some steam was provided for the completion of cooking.

Most of the above processes require sophisticated equipment with a steaming chamber and moving belt type mechanisms for rice handling. Further, in the previously proposed hardware, a scheme for the recovery of sensible enthalpy was not included. Therefore, in the present work, an attempt has been made to eliminate both of these limitations.

5.2. Equipment. The continuous cooker consists of two sections: (a) cooking and (b) heat recovery. It is schematically shown in Figure 21. Both sections consist of a U-trough with a single screw (primary screw) for moving the material in the forward direction. The trough has a jacket for providing the heat through condensing steam. Heat can also be supplied by open steam injected through nozzles. The speed of rotation of the screw can be adjusted through a variable frequency drive (VFD) attached to a motor. Rice or lentils or a mixture of both are fed through a hopper. The cooked material overflows from the trough through an opening at the far end with an adjustable screw arrangement (secondary screw weir for maintaining the water level inside the trough and for positive displacement of cooked material). The cooked material falls into a heat recovery unit having practically the same arrangement as the cooking section except that the jacket is replaced by a limped coil. In addition, the steam nozzles are absent in the heat recovery section. Cooking experiments were

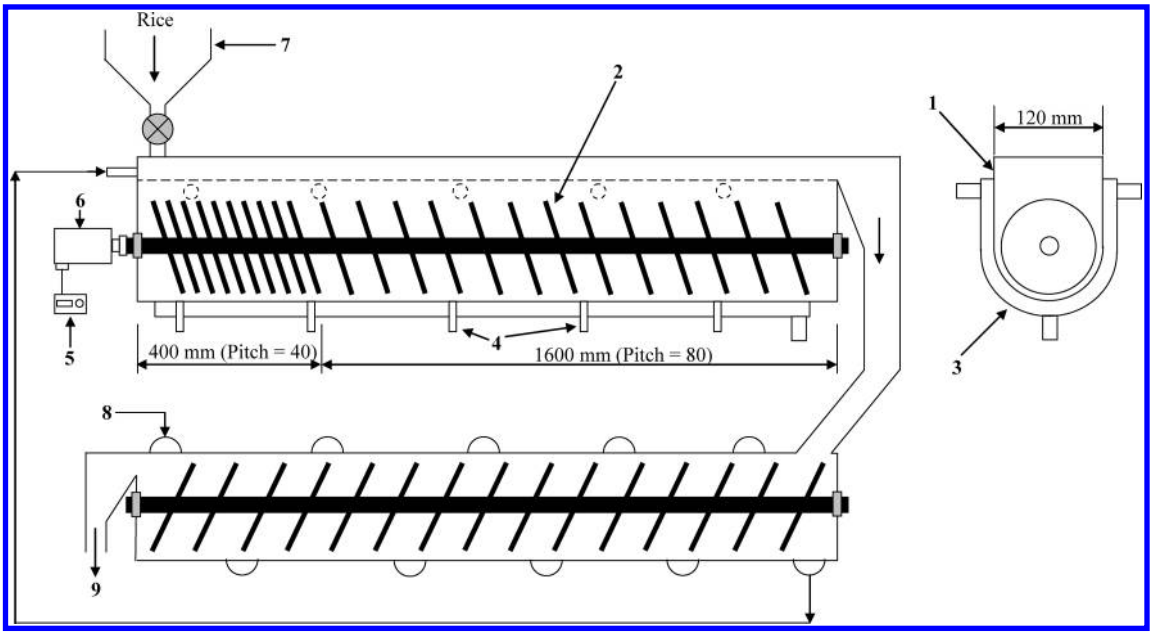

Figure 21. Schematic of continuous cooking equipment: (1) U-trough, (2) single screw for moving material in forward direction, (3) jacket for condensing steam, (4) nozzles for direct steam injection, (5) variable frequency drive, (6) motor, (7) hopper for addition of rice/lentils, (8) limped coil, (9) rice/lentils outlet.

performed with a screw diameter of 108 mm and length of 1850 mm with a central shaft of 33 mm diameter. Total length of the trough is 2000 mm and width is 120 mm. The pitch of the screw is 40 mm for the initial 400 mm length and 80 mm for the rest of the screw length. As shown from the schematic (Figure 21), the trough extends above the screw for accommodating extra water if necessary. A rectangular plate with two handles on the top surface and hinges on one side are provided to cover the trough from above. The cover arrangement is handy during cleaning operation.

Because the cooked rice was to be removed from the equipment in suspended form, initial trials were carried out to understand the effect of speed of rotation of the screw. A higher speed would result in the breakage of cooked rice, while a very low speed can result in improper suspension. In the first trial, 30 kg of water was charged and brought to the boiling point, and then rice was charged from the feed end with screws rotating at 0.5 r/s. It was observed that the rice grains moved gradually along the length of the trough. A sample of rice water slurry was removed from the other end. From the samples collected, it was found that cooked rice started coming out after an average residence time of about 25 min.

Though the rice was cooked completely, there was large breakage of grains indicating the need to lower the speed of rotation. In another trial, the rotation speed was decreased to 0.4 r/s with rice addition of 10 kg at the start, followed by 2 kg/h on a continuous basis. Samples of rice coming out from the discharge end were continuously checked for cooking, and the rice was found to be cooked satisfactorily During the final trial, the speed of rotation was further reduced to 0.25 r/s. Ten kilograms of rice was charged initially in heated water, and further addition was continued at the rate of 13 kg/h. Considering that rice requires water in the proportion of approximately 1:2.5 for cooking and some water is required for suspension, water was charged at the rate of 71 kg/h. The operation was carried out for 2 h. Rice coming out after the initial 20 min time was found to be cooked nicely. The ratio of cooked rice to free water was found to be 1:3. It was concluded from these trials that a residence time of 20 min was sufficient for cooking of rice.

The construction and the performance evaluation of the heat recovery unit is in progress. In one trial the flow rate of ambient water was 60 kg/h, ambient water enters at (30 ± 1 °C), and the hot water leaves at about (83 °C). The cooked rice leaves at about (50 °C) and is ready for continuous packaging. The overall heat balance indicates that 70% of the sensible enthalpy can be recovered in the form of hot water, which in turn can be added to the feed rice. In reality, the sensible enthalpy needed for cooking has been provided to increase the temperature of inlet water and rice (~30 °C) to the outlet cooked rice temperature of 50 °C. Thus, the energy requirement compared with the efficient batch operation (Section 3) is about 45%. It may be further noted that the batch operation reached 70% thermal efficiency compared with the range of 10−20% obtained in the conventional open pan cooking. It is interesting to note that for the estimation of efficiency (eq 1), the denominator is the amount of enthalpy to heat the material (rice and water) from 30 to 100 °C. Because we have recovered 70% of this heat, the energy needed in the continuous process is about 12−15 times lower than the conventional open pan cooking. This is a significant result. Considering the enormous potential of a continuous cooker, further work is in progress for the scale-up and development of a reliable procedure for large scale cooking.

6. CONCLUSIONS

(1) Efficient designs for cooking systems have been developed using LPG with sizes of 4, 6, 24, 30, 72, 120, 160, and 700 L, catering to the food needs for people in the range of 6− 2000.

(2) The cooking pots gain energy from condensing steam on the outside surface. The cooking charge (water + rice or lentils and/or vegetables) receive heat by the mode of natural convection. The flow and temperature pattern has

been analyzed by computational fluid dynamics (CFD). The CFD prediction and experimental measurements indicate that the optimum heat flux (on the basis of LPG burning) is in the range of 16,000−25,000 kCal/h m^2, where m^2 is the bottom surface area of the cooking system.

(3) The heat losses to the surroundings have been reduced by providing air gap insulation between the covers. The flow pattern in the air gap has been comprehensively analyzed by computational fluid dynamics. The optimization has shown that the air gap should be in the range of 10−12 mm.

(4) The optimum gap between the burner top and the cooker bottom was found to be 3 mm for all cooking systems covered in this work. For instance, for a 6 L cooker, an increase in the gap to 7, 12, and 15 mm reduces the thermal efficiency by 14, 22, and 23%, respectively. Further, it was also found that the effect of the gap was found to be relatively less severe when the cooker size is increased. Thus, an increase from a 3 to 6 mm gap results in a reduction in thermal efficiency of 5% compared to about 10% for a 6 L cooker.

(5) The cooking reaction is practically thermally neutral. Therefore, when the contents are heated to boiling temperatures, the energy supply can be stopped by switching off the fuel supply. After this point, the temperature was found to decrease by less than 5 °C in 30 min. This is because of the quality of insulation provided by the air gap and the loss of contact between the water in the container vessel and the bottom pot. Thus, after the fuel shut off, the temperature of cooking material remains above the cooking temperature.

(6) The combined effect of all of the optimization exercises has given a value of thermal efficiency in the range of 65−75% and useful efficiency in the range of 50−60%. These efficiencies have been explained in eq 1 in Part I. It is noted that conventional cooking methods give thermal efficiencies in the range of 10−20%.

(7) More than 50 cookers (72−160 L) are in actual practice at various locations. LPG consumption has found to be reduced by about 60%.

(8) At present, the cost of a cooker is about U.S. $630, which caters the food for about 300 people. With 20% depeciation and 10% interest on capital cost, the pay out period works out to be eight months at a LPG price of 44 cents per kg.

7. SUGGESTIONS FOR FUTURE WORK

(a) Simulations using computational fluid dynamics is discussed in Section 2. The work needs to be extended for detailed analysis of temperature and flow patterns in cooking pots. Investigations are needed to understand the sensitivity of pot diameter, extent of filling, ratios of rice/lentils/vegetables to water, and the extent of cooking. It may be pointed out that the porosity, average particle size, and level of cooked material change with respect to time. The CFD simulations need to take into account the flow through porous media with variable thickness. Further, the extraction of starch in water may import viscous or non-Newtonian behavior to the liquid phase, and the description of interface forces need to be described accordingly[39]. Detailed analysis needs to be carried out regarding temperature stratification. This information should enable development of suitable internals so the extent of stratification be reduced to permit cooking at all the locations. This exercise will also allow for the maximization of the size of the cooking pot, and hence, reduce the number of pots required, which will lessen the drudgery for cooking personnel.

(b) On the basis of mathematical modeling and CFD analysis, we need to find the flow and turbulent structures.[40−53] It is known that such information is useful for understanding the transport phenomenon in general and heat transfer in particular. The later is useful in the present work.

(c) The flow pattern around the particle should also be investigated using computational fluid dynamics with direct numerical simulation (DNS).[54]

(d) It is shown in Section 2.3 that the heat flux absorbed by the cooking pot diminishes as the temperature approaches boiling point. For implementing this observation, a control strategy needs to be devised that shall be simple in construction and operation.

(e) In regard to use of solid fuels, substantial additional work is needed to achieve desired burning rate over a sustained period. Rational procedures need to be developed for optimum design and scale-up.

(f) Section 3 brought out the huge potential in continuous cooking. Additional work is needed to attain free flow of solids until outlet. We need to measure residence time distribution of solid phase for attaining near plug flow. An attempt needs made for optimization of energy utilization, which means partial cooking of cooked food against preheating of water.

(g) It will prove useful to undertake a systematic investigation of the conventional cooking practices (as many as possible from different countries) for measurement of thermal and useful efficiencies.

(h) In order to establish the amount of heat actually used for the cooking reaction, systematic research work is needed for estimating the heat of the cooking reactions for the variety of materials being cooked in practice.

(i) The implementation of improved cooking systems developed in this work is expected to have substantial impact on the energy footprint of developing countries. Success will lie in the dissemination of knowledge and large scale implementations. For this purpose, concerted efforts are needed with strong collaboration between scientific institutions, NGOs, and governments.

AUTHOR INFORMATION

Corresponding Author

*Phone: +91 22 33611111 (J.B.J). Fax: +91 22 33611020 (J.B.J). E-mails: jbjoshi@gmail.com (J.B.J), ab.pandit@ictmumbai.edu.in (A.B.P.), shirish@spacpl.com (S.B.P.).

Present Addresses

⊥AISSMS College of Engineering, Pune −411001, India

NOTATIONS

A = area of heat transfer (m^2)
AR = aspect ratio (H/L) (−)
A_0 = pre-exponential constant in eq 14 (s^{-1})
C = quantitative value of the product of degradation under consideration (mol L^{-1})
$[C]_0$ = value of the product under consideration at time 0 (mol L^{-1})

$[C]_t$ = value of the product under consideration after reaction time t (mol L^{-1})
ΔC = amount degraded during t_i (mol L^{-1})
C_P = specific heat capacity (kJ kg^{-1} K^{-1})
CV = calorific value (kJ kg^{-1})
D = diameter of pot/cooking vessel (m)
Ea = activation energy of the reaction (J mol^{-1})
f_β = constant as in Table 1
G_b = generation of turbulence due to buoyancy (m^4 s^{-1})
G_k = generation of turbulence kinetic energy due to mean velocity gradients (kg $m^{-1}s^3$)
G_ω = production of ω
g = gravitational constant (m s^{-2})
H = height of the pot/Cooking vessel (m)
H_E = height of the enclosure (m)
h_i = inside heat transfer coefficient (W m^{-2} K^{-1})
h_{ins} = time-averaged inside heat transfer coefficient (W m^{-2} K^{-1})
h_o = outside heat transfer coefficient (W m^{-2} K^{-1})
I = turbulence intensity (%)
k = turbulent kinetic energy per unit mass (m^2 s^{-2})
k_t = thermal conductivity (W m^{-1} K^{-1})
k_1 = reaction rate constant (s^{-1})
k_i = rate constant at time t_i (s^{-1})
L = gap width of enclosure (m)
M = mass (kg)
m = quantity of steam evaporated (kg)
n = order of the reaction
Nu = Nusselt number (−)
p = pressure (Pa)
R = ideal gas constant (Jmol^{-1} K^{-1})
Ra = Rayleigh number ($g\beta\Delta TW^3/\nu\alpha$) (−)
S = stratification number (−)
$|\overline{S}|$ = mean strain rate (s^{-1})
$\overline{Sij}$ = strain rate (s^{-1})
T = temperature (K)
T_C = temperature of the outer cover (K)
T_H = temperature of inner cover (K)
T_0 = reference temperature (K)
T_{max} = maximum temperature of fluid (K)
T_{min} = minimum temperature of fluid (K)
t = time (s)
$\langle\Delta T\rangle$ = average temperature driving force (K)
U = overall heat transfer coefficient (W m^{-2} K^{-1})
u_r = mean radial velocity (m s^{-1})
u_z = mean axial velocity (m s^{-1})
$\langle u\rangle$ = time averaged mean velocity (m s^{-1})
u_θ = mean annular velocity (m s^{-1})
u = horizontal velocity (m.s^{-1})
V_1 = standard pot/vessel
V_2 = tall pot/vessel
V_3 = standard pot/vessel
V_4 = tall pot/vessel
V_{en} = enclosed volume (m^3)
X = amount of rice (kg)
x = abscissa (m)
Y = ratio of water to rice (kg/kg)
Y_k = dissipation of turbulent kinetic energy (s^{-1})
y = ordinate (m)

Greek Symbols

α = thermal diffusivity (m^2 s^{-1})
α_{eff} = effective thermal diffusivity (m^2 s^{-1})
$\alpha_{\infty,1}$ = constant in Table 1
$\alpha_{\infty,2}$ = constant in Table 1
β = coefficient of thermal expansion (K^{-1})
β_r = constant in Table 1
β^*_∞ = constant in Table 1
ρ = density of fluid (kg m^3)
ρ_0 = density of fluid at reference temperature (kg m^3)
Δ = difference in quantity, e.g., temperature
ε = turbulent kinetic energy dissipation rate per unit mass (m^2 s^{-3})
λ = latent heat of vaporaization (kJ kg^{-1})
μ = viscosity (m^2 s^{-1})
μ_t = turbulent viscosity (m^2 s^{-1})
μ_{eff} = effective viscosity of fluid (m^2 s^{-1})
ν_t = turbulent kinematic viscosity (m^2 s^{-1})
ω = specific dissipation rate (s^{-1})
σ_k = turbulent Prandtl number for energy dissipation rate (−)
σ_t = turbulent Prandtl number for kinetic energy (−)
χ_k = constant in Table 1
η = efficiency

Subscripts

B = quantity in base
C = contents
G = LPG gas
i = inner diameter
lm = logarithmic mean
o = outer diameter
therm = thermal
use = useful
V = vessel
W = water

Abbreviations

CFD = computational fluid dynamics
DNS = direct numerical simulation
SS = stainless steel

REFERENCES

(1) Legros, G.; Havet, I.; Bruce, N.; Bonjour, S. The Energy Access Situation in Developing Countries. WHO and UNDP, 2009. http://www.who.int/indoorair/publications/energyaccesssituation/en/index.html (accessed January 3, 2012).
(2) Wikipedia. http://wiki.answers.com/Q/What_percentage_of_the_world's_population_lives_in_developing_countries (accessed January 3, 2012).
(3) Ganguli, A. A.; Pandit, A. B.; Joshi, J. B. CFD simulation of heat transfer in a two-dimensional vertical enclosure. *Chem. Eng. Res. Des.* **2009**, *87*, 711–727.
(4) Ganguli, A. A.; Sathe, M. J.; Pandit, A., B.; Joshi, J. B.; Vijayan, P. K. Hydrodynamics and heat transfer characteristics of passive decay heat removal systems: CFD simulations and experimental measurements. *Chem. Eng. Sci.* **2010**, *65*, 3457–3473.
(5) Reddy, R. K.; Joshi, J. B. CFD modeling of solid-liquid fluidized beds of mono and binary particle mixtures. *Chem. Eng. Sci.* **2009**, *64*, 3641–3658.
(6) Batchelor, G. K. Heat transfer by free convection across a closed cavity between vertical boundaries at different temperatures. *Q. Appl. Math.* **1954**, *12*, 209–233.
(7) Elder, J. W. Laminar free convection in a vertical slot. *J. Fluid Mech.* **1965**, *23*, 77–98.
(8) Yin, S. H.; Wung, T. Y.; Chen, K. Natural convection in an air layer enclosed within rectangular cavities. *Int. J. Heat Mass Transfer* **1978**, *21*, 307–315.

(9) Elsherbiny, S. M.; Raithby, G. D.; Hollands, K. G. T. Heat transfer by natural convection across vertical and inclined air layers. *Trans. ASME, J. Heat Transfer* **1982**, *104*, 96–102.
(10) Wakitani, S. Experiments on convective instability of large Prandtl number fluids in a vertical slot. *J. Fluid Mech.* **1994**, *116*, 120–126.
(11) Newell, M. E.; Schmidt, F. W. Heat transfer by laminar natural convection within rectangular enclosures. *Trans. ASME, Ser. C* **1970**, *92*, 159–167.
(12) Korpela, S. A.; Lee, Y.; Drummond, J. E. Heat transfer through a double pane window. *Trans ASME, J. Heat Transfer* **1982**, *104*, 539–544.
(13) Lee, Y.; Korpela, S. Multicellular natural convection in a vertical slot. *J. Fluid Mech.* **1983**, *126*, 91–124.
(14) Le Quéré, P. A note on multiple and unsteady solutions in two-dimensional convection in a tall cavity. *Trans. ASME, J. Heat Transfer* **1990**, *112*, 965–973.
(15) Wakitani, S. Formation of cells in natural convection in a vertical slot at large Prandtl number. *J. Fluid Mech.* **1996**, *314*, 299–314.
(16) Wakitani, S. Development of multicellular solutions in natural convection in an air-filled vertical cavity. *Trans. ASME, J. Heat Transfer* **1997**, *119*, 97–101.
(17) Zhao, Y.; Curcija, D.; Gross, W. P. Prediction of multicellular flow regime of natural convection in fenestration glazing cavities. *ASHRAE Trans.* **1997**, *103*, 1–12.
(18) Lartigue, B.; Lorente, S.; Bourret, B. Multicellular natural convection in high aspect ratio cavity: Experimental and numerical results. *Int. J. Heat Mass Transfer* **2000**, *43*, 3157–3170.
(19) Ekambara, K.; Joshi, J. B. CFD Simulation of flow in bubble columns: Laminar and transition regimes. *Ind. Eng. Chem. Res.* **2005**, *44*, 1413–1423.
(20) Thakre, S. S.; Joshi, J. B. CFD simulation of bubble column reactor: Importance of drag force formulation. *Chem. Eng. Sci.* **2001**, *56*, 5893–5933.
(21) Incropera, F. P.; Dewitt, D. P. *Fundamentals of Heat and Mass Transfer*, 5th ed.; Wiley & Sons: NewYork, 2005.
(22) *User's Manual to FLUENT 6.2*; Fluent, Inc.: Centrera Resource Park, Lebanon, NH, 2005.
(23) Gandhi, M.; Sathe, M. J.; Joshi, J. B.; Vijayan, P. K. Two phase natural convection: CFD simulations and PIV measurement. *Chem. Eng. Sci.* **2011**, *66*, 3152–3171.
(24) Aszodi, A.; Krepper, E.; Presser, H. M. *Investigation of Heating up and Evaporation Processes of Fluids in Storage Tanks by Experiments and by Numerical Simulation*. Second International Symposium on Two Phase Flow Modeling and Experimentation, Pisa Proceedings, 2000, pp 1667−1674.
(25) Kang, M. Thermal mixing in a water tank during heating process. *Int. J. Heat Mass Transfer* **2002**, *45*, 4361–4366.
(26) Krepper, E.; Hicken, E. F.; Jaegers, H. Investigation of natural convection in large pools. *Int. J. Heat Fluid Flow* **2002**, *23*, 359–365.
(27) Calcagni, B.; Marshili, F.; Paroncini, M. Natural convective heat transfer in square enclosures heated from below. *Appl. Therm. Eng.* **2005**, *25*, 2552–2531.
(28) Sharma, A., K.; Velusamy, K.; Balaji, C. Turbulent natural convection in an enclosure with localized heating from below. *Int. J. Heat Mass Transfer* **2007**, *46*, 1232–1241.
(29) Han, Y. M.; Wang, R. Z.; Dai, Y. J. Thermal stratification within the water tank. *Renewable Sustainable Energy Rev.* **2009**, *13*, 1014–1026.
(30) Reddy, R. K.; Joshi., J. B. CFD modeling of pressure drop and drag coefficient in fixed beds: Wall effects. *Particuology* **2010**, *8*, 37–43.
(31) BIS Sandard: IS 5116, 1996.
(32) George, R. *Solar Cooking for Healthy Living- Solar Cooker: A Device for Nutritious Food*; Faculty of Home Science, The M.S. University of Baroda, Vadodara, India, 2001.
(33) Danao, S. P.; Joshi, J. B. Solar Cooking: Optimisation of Paraboloidal Concentrator. *Proc. Indian Natl. Sci Acad.* **2011**, *77* (4), 373–388.
(34) Danao, S. P.; Joshi, J. B. Optimisation of Solar Box Cooker. *Proc. Indian Natl. Sci Acad.* **2011**, *77* (1), 1–18.
(35) Scheffler, W. Introduction to the Revolutionary Design of Scheffler Reflectors. Solar Cooker International Conference, 2006. http://www.docstoc.com/docs/100239025/Introduction-to-the-Revolutionary-Design-of-Scheffler-Reflectors (accessed January 4, 2012).
(36) Sugimura, T. Process for Continuous Rice Cooking by Steaming and Apparatus Thereof. U.S. Patent 4571341, 1986.
(37) Watanabe, K. Automatic and Continuous Rice Cooking System. U.S. Patent 4934259, 1990.
(38) Miyagawa, T.; Ishii, Y.; Tanaka, T. Method and apparatus for continuously steaming and boiling rice. U.S. Patent 6056986, 2000.
(39) Lali, A. M.; Khare, a.S.; Joshi, J. B.; Nigam, K. D. P. Behavior of solid particles in viscous non Newtonian solutions: settling velocty, Wall effects and bed expansion in solid liquid fluidized beds. *Powder Technol.* **1989**, *57*, 39–50.
(40) Joshi, J. B.; Ranade, V. V.; Gharat, S. D.; Lele, S. S. Sparged loop reactors. *Can. J. Chem. Eng.* **1990**, *68*, 705–741.
(41) Joshi, J. B. Computational flow modeling and design of bubble column reactors. *Chem. Eng. Sci.* **2001**, *5*, 5893–5933.
(42) Tabib, M. V.; Roy, S. V.; Joshi, J. B. CFD simulation of bubble columns: an analysis of interface force and turbulence models. *Chem. Eng. J.* **2008**, *139*, 589–614.
(43) Bhole, M. R.; Joshi, J. B.; Ramakrishna, D. CFD simulation of bubble columns incorporating population balance modeling. *Chem. Eng. Sci.* **2008**, *63*, 2267–2282.
(44) Dijkhuizen, W.; Roghair, I.; Van Sint Annaland, M.; Kuipers, J. A. M. DNS of gas bubbles behaviour using an improved 3D front tracking model: Model development. *Chem. Eng. Sci.* **2010**, *65*, 1427–1437.
(45) Dijkhuizen, W.; Van Sint Annaland, M.; Kuipers, J. A. M. Numerical and experimental investigation of the lift force on single bubbles. *Chem. Eng. Sci.* **2010**, *65*, 1274–1287.
(46) Joshi, J. B.; Sharma, M. M. Mass transfer characteristic of horizontal sparged contactors. *Trans. Inst. Chem. Eng.* **1976**, *54*, 42–53.
(47) Joshi, J. B.; Sharma, M. M. Liquid phase backmixing in sparged contactors. *Can. J. Chem. Eng.* **1978**, *56*, 116–119.
(48) Joshi, J. B.; Vitankar, V. S.; Kulkarni, A. A.; Dhotre, M. T.; Ekambara, K. Coherent flow structures in bubble column reactors. *Chem. Eng. Sci.* **2002**, *57*, 3157–3183.
(49) Mathpati, C. S.; Joshi, J. B. Insight into theories of heat and mass transfer at solid−fluid interfaces using direct numerical simulation and large eddy simulation. *Ind. Eng. Chem. Res.* **2007**, *46*, 8525–8557.
(50) Tabib, M. V.; Joshi, J. B. Analysis of dominant flow structures and their flow dynamics in industrially relevant equipment using proper orthogonal decomposition. *Chem. Eng. Sci.* **2008**, *63*, 3695–3715.
(51) Deshpande, S. S.; Joshi, J. B.; Kulkarni, V. R.; Kulkarni, B. D. Identification and characterization of flow structures in chemical process equipment using multi-resolution techniques. *Chem. Eng. Sci.* **2008**, *63*, 5330–5346.
(52) Joshi, J. B.; Tabib, M. V.; Deshpande, S. S.; Mathpati, C. S. Dynamics of flow structures and transport phenomena. I. Experimental and numerical techniques for identification and energy content of flow structures. *Ind. Eng. Chem. Res.* **2009**, *48*, 8244–8284.
(53) Mathpati, C. S.; Tabib, M. V.; Deshpande, S. S.; Joshi, J. B. Dynamics of flow structures and transport phenomena. II. Relationship with design objectives and design optimization. *Ind. Eng. Chem. Res.* **2009**, *48*, 8285–8311.
(54) Reddy, R. K.; Jin, S.; Nandakumar, K.; Minev, P. D.; Joshi, J. B. Direct numerical simulation of free falling spheres in creeping flow. *Int. J. Comp. Fluid Dyn.* **2010**, *24*, 109–120.